

The SOPHIE search for northern extrasolar planets ★,★★

V. Follow-up of ELODIE candidates: Jupiter-analogues around Sun-like stars

I. Boisse^{1,2}, F. Pepe³, C. Perrier⁴, D. Queloz³, X. Bonfils⁴, F. Bouchy^{2,5}, N.C. Santos^{1,6}, L. Arnold⁵, J.-L. Beuzit⁴, R.F. Díaz⁷, X. Delfosse⁴, A. Eggenberger⁴, D. Ehrenreich⁴, T. Forveille⁴, G. Hébrard^{2,5}, A.M. Lagrange⁴, C. Lovis³, M. Mayor³, C. Moutou⁷, D. Naef³, A. Santerne⁷, D. Ségransan³, J.-P. Sivan⁷, and S. Udry³

¹ Centro de Astrofísica, Universidade do Porto, Rua das Estrelas, 4150-762 Porto, Portugal
e-mail: Isabelle.Boisse@astro.up.pt

² Institut d'Astrophysique de Paris, UMR7095 CNRS, Université Pierre & Marie Curie, 98bis Bd Arago, 75014 Paris, France

³ Observatoire de Genève, Université de Genève, 51 Ch. des Maillettes, 1290 Sauverny, Switzerland

⁴ Université Joseph Fourier – Grenoble 1 / CNRS, Laboratoire d'Astrophysique de Grenoble (UMR 5571), BP 53, 38041 Grenoble Cedex 9, France

⁵ Observatoire de Haute Provence, CNRS/OAMP, 04870 St Michel l'Observatoire, France

⁶ Departamento de Física e Astronomia, Faculdade de Ciências, Universidade do Porto, Rua do Campo Alegre, 4169-007 Porto, Portugal

⁷ Laboratoire d'Astrophysique de Marseille, Université de Provence & CNRS, 38 rue Frédéric Joliot-Curie, 13388 Marseille cedex 13, France

Received XX; accepted XX

ABSTRACT

We present radial-velocity measurements obtained in one of the programs to search for extrasolar planets with the spectrograph SOPHIE at the 1.93-m telescope of the Haute-Provence Observatory. Targets were selected from catalogs observed with ELODIE, mounted previously at the telescope, in order to detect long-period planets with an extended database close to 15 years.

Two new Jupiter-analogue candidates are reported to orbit the bright stars HD150706 and HD222155 in 16.1 and 10.9 yr at $6.7^{+4.0}_{-1.4}$ and $5.1^{+0.6}_{-0.7}$ AU. They respectively have minimum masses of $2.71^{+1.44}_{-0.66}$ and $1.90^{+0.67}_{-0.53} M_{Jup}$. Using the measurements from ELODIE and SOPHIE, we refine the parameters of the long-period planets HD154345b and HD89307b, and publish the first reliable orbit for HD24040b. This last companion has a minimum mass of $4.01 \pm 0.49 M_{Jup}$ orbiting its star in 10.0 yr at 4.92 ± 0.38 AU. Moreover, the data present evidence for a third bound object in the HD24040 system.

With a surrounding dust debris disk, HD150706 is an active G0 dwarf for which we partially corrected the effect of the stellar spot on the SOPHIE radial-velocities. By contrast, HD222155 is an inactive G2V. In the SOPHIE measurements an instrumental effect could be characterized and partly corrected. Considering the work of Lovis et al. (2011b) and that we did not find significant correlation with the activity index in the SOPHIE data, the radial-velocity variations are not expected to come from stellar magnetic cycles. Finally, we discuss the main properties of this new population of long-period Jupiter-mass planets, for the moment, builds up of less than 20 candidates. These stars are preferential targets for direct-imaging or astrometry follow-up to constrain the system parameters and for higher precision radial-velocity to search for lower mass planets, aiming to find a Solar System twin. In the Appendix, we determine the relation that gives the radial-velocity offset between the ELODIE and SOPHIE spectrographs.

Key words. planetary systems – techniques: radial velocimetry – stars: individual: HD 222155, HD 150706 ,HD 24040, HD 154345, HD 89307– magnetic cycle

1. Introduction

Our search for planetary systems is partly motivated to put in perspective the Solar System and to understand its formation. Until now, most of the discovered systems have not resembled the planets of our System. If we observe the Sun in radial-velocity (hereafter RV), the main signature should be that of Jupiter with a period of 11.86 yr, an orbital distance of 5.2 AU and a RV semi-amplitude of about 12 ms^{-1} . The detection of

long-period Jupiter-like planets are expected to be the first step in the quest for an analog of the Solar System. This step is already achievable, in contrast to the earth-like planets in the habitable zone of their host stars that will generally need the next generation of instruments.

Recently, the long-term accuracy of several spectrographs and the timescale of some RV surveys begin to allow discoveries of long-period planets. Few planets are known to date within the orbital distance range of Jupiter with less than seventeen planets orbiting at distance greater than 4 AU (cf. Table 1). Some of them were announced with incomplete orbits. These planets overlap with the few microlensing detections at such orbital distances and in the Jupiter-mass regime: OGLE235-MOA53b is a $2.6 M_{Jup}$ planet at 5.1AU (Bond et al. 2008) and OGLE-2008-BLG-513/MOA-2008-BLG-401b, a $6.8 M_{Jup}$ orbiting at 4

* Based on observations made with the ELODIE and the SOPHIE spectrographs on the 1.93-m telescope at Observatoire de Haute-Provence (OHP, CNRS/OAMP), France (program 07A.PNP.CON) and on spectral data retrieved from the ELODIE archive at OHP.

** Tables C.1 to 10 are only available in electronic form at the CDS via anonymous ftp to cdsarc.u-strasbg.fr (130.79.128.5) or via <http://cdsweb.u-strasbg.fr/cgi-bin/qcat?J/A+A/>

AU from its star (Yee et al. 2011). We note that the planet-host stars are expected to be low-mass stars and their giant planets are colder than Jupiter.

The SOPHIE Consortium began a large program to search for planets in October 2006 (Bouchy et al. 2009) that led to several planet discoveries (e.g. Hébrard et al. 2010, Boisse et al. 2010b, Díaz et al. 2011). Among the different subprograms, one focuses on the follow-up of the drifts and long-period signals detected in the ELODIE sample, in continuity of the historical program begun by M. Mayor and D. Queloz in 1994 with the spectrograph ELODIE during more than 12 years (Mayor & Queloz 1995; Naef et al. 2005). These trends are identified as incomplete orbits of gravitationally bound companions and the monitoring aims to determine their periods and their masses (and thus the planet/brown dwarf/star nature). The SOPHIE spectrograph replaces ELODIE at the 1.93m-telescope at Observatoire de Haute-Provence (OHP) since October 2006. About 40 targets were selected from the original ELODIE catalog (that contained about 400 targets). They are mainly G and K dwarfs to be followed-up with SOPHIE with the objective to detect very long period planets (>8 yr) and multiple systems.

We report the detection of two Jupiter-analogues around the Sun-like stars HD150706 and HD222155 thanks to ELODIE and SOPHIE RV measurements. The observations are presented in Section 2. We then characterize the planet-host stars. In a fourth section, we analyze the RV measurements and constrain the planetary parameters. In a fifth section, we determine the first reliable orbit for HD24040b (Wright et al. 2007), and refine the planetary parameters of HD154345b (Wright et al. 2008) and HD89307b (Fischer et al. 2009). At last, we discuss that the observed RV variations should not come from long-term magnetic cycles, before putting these new planets in the context of the other discoveries and the perspectives for these systems to be followed. In the Appendix, we parameter the RV shift between the ELODIE and SOPHIE data.

2. Radial velocity measurements

Measurements were obtained with the cross-dispersed echelle ELODIE spectrograph mounted on the 1.93-m telescope at the Observatoire de Haute-Provence observatory (OHP, France) between late 1993 and mid 2006 (Baranne et al. 1996). The stars were then monitored by the SOPHIE spectrograph that replaced ELODIE with improved capabilities in terms of stability, limiting magnitude, and resolution. For the two instruments, the stellar spectrum were recorded simultaneously with a thorium-argon calibration (thosimult mode, Bouchy et al. 2009) allowing an estimation of the intrinsic drift of the spectrograph at the same time that the observation. The optical fibers include a double scrambler in the path of light to improve the RV stability. A mean time exposure of 900 s (that is allowed to vary between 600 and 1200s as a function of the weather conditions) reduces the photon noise and averages the acoustic oscillation modes (p-modes).

ELODIE has a resolving power $R=\lambda/\Delta\lambda \approx 42\,000$ (at 550 nm, see e.g. Perrier et al. 2003 for more details). The spectra are correlated with a G2-spectral type numerical mask. The resulting cross-correlation functions (CCF) are fitted by Gaussians to derive the RV values (Baranne et al. 1996, Pepe et al. 2002).

The SOPHIE observations were performed in high-resolution mode reaching a resolution power of $\Delta\lambda/\lambda \approx 75\,000$ (at 550 nm). The SOPHIE automatic data reduction software was used to derive the RV from the spectra, after a cross-correlation with a G2-spectral type numerical mask (Baranne et al. 1996;

Pepe et al. 2002) and a fit of a Gaussian on the CCF. The typical photon-noise uncertainty is around 1.5 ms^{-1} (calculated as described in Boisse et al. 2010b). But the main error source on these measurements is coming from the instrument, the *seeing effect* (Boisse et al. 2010a,b). This instrumental effect is due to bad scrambling of one multimode fiber that leads to non-uniform illumination of the entrance of the spectrograph. We note that this noise has been removed thanks to a fiber link modification which includes a piece of octagonal-section fiber in June 2011 (Perruchot et al. 2011). An external systematic error of 4 ms^{-1} for instrumental errors (guiding, centering and seeing) was then quadratically added to the SOPHIE mean measurement uncertainty. Seeing error is not expected in the ELODIE measurements as the instrumental configuration was different, but the RV uncertainty take into account the guiding and centering errors. In the following, the signal-to-noise ratio (SNR) are given per pixel at 550 nm. We note the sampling per resolution element (FWHM) is of 2.2 pixels for ELODIE and of 2.7 pixels in the high-resolution mode for SOPHIE.

The RV data are available at the CDS in the given Tables, that contain in theirs cols. 1-3, the time of the observation (barycentric Julian date), the RV, and its error, respectively

2.1. HD150706

During 9 years, between July 1997 and June 2006, 50 RV measurements were done with the ELODIE spectrograph. We did not take into account two measurements with $\text{SNR}<10$. SOPHIE obtained 59 observations of HD150706 between May 2007 and April 2011. Five measurements with SNR lower than 100 were removed. One spectrum contaminated by moonlight was also discarded. The final data set contains 48 ELODIE and 53 SOPHIE measurements with a typical SNR of, respectively, 80 and 172. The data are available at the CDS in Tables A.1 (ELODIE) and A.2 (SOPHIE).

2.2. HD222155

We obtained 44 spectra of HD222155 with the ELODIE spectrograph on a timescale of 8 years between August 1997 and November 2005. HD222155 was observed 71 times by SOPHIE between July 2007 and January 2011. Three measurements with SNR lower than 100 were removed. One observation made with the background sky spectrum recorded simultaneously (*objAB* mode, Bouchy et al. 2009) in order to measure the stellar parameters (cf. Sect. 3.2) was discarded. The final data set comprises 44 ELODIE measurements with a typical SNR of 92 and 67 SOPHIE values with a mean SNR of 173. The data are available at the CDS in Tables A.3 (ELODIE) and A.4 (SOPHIE).

3. Planet host stars

3.1. HD150706

HD150706 (HIP80902) is a G0V star with an apparent Johnson V-band magnitude of $m_V=7.0$ (Hipparcos catalogue, ESA 1997). With an astrometric parallax of $\pi=35.43\pm 0.33\text{ mas}$ (van Leeuwen 2007), we derived a distance of $28.2\pm 0.3\text{ pc}$, that leads to an absolute V-band magnitude of 4.75. A stellar diameter $R_\star=0.96\pm 0.02R_\odot$ is estimated by Masana et al. (2006) from photometric measurements.

A spectroscopic analysis (Santos et al. 2004) was done on high-resolution spectra obtained with the UES spectrograph on the 4-m William Herschel telescope (Santos et al. 2003). They

Table 2. Stellar parameters for HD 150706 and HD 222155.

Parameters	HD 150706	HD 222155
Sp. T.	G0V	G2V
m_V	7.0	7.1
B - V	0.57	0.64
π [mas]	35.43 ± 0.33	20.38 ± 0.62
T_{eff} [K]	$5961 \pm 27^{(1)}$	$5765 \pm 22^{(2)}$
$\log g$ [cgs]	$4.5 \pm 0.1^{(1)}$	$4.10 \pm 0.13^{(2)}$
Fe/H [dex]	$-0.01 \pm 0.04^{(1)}$	$-0.11 \pm 0.05^{(2)}$
$v \sin i_*$ [km s ⁻¹]	$3.7 \pm 1.0^{(3)}$	$3.2 \pm 1.0^{(3)}$
M_* [M_\odot]	$1.17 \pm 0.12^{(1)}$	1.13 ± 0.11
R_* [R_\odot]	0.96 ± 0.02	1.67 ± 0.07
$\log R'_{\text{HK}}$ [dex]	$-4.47 \pm 0.10^{(3)}$	$-5.06 \pm 0.10^{(3)}$
Age [Gyr]	1-5	8.2 ± 0.7
Distance [pc]	28.2 ± 0.3	49.1 ± 1.5

⁽¹⁾ Parameter derived from the UES spectra (Santos et al. 2003).

⁽²⁾ Parameter derived from the SOPHIE spectrum (Santos et al. 2004).

⁽³⁾ Parameter derived from the SOPHIE CCF (Boisse et al. 2010b).

derived an effective temperature $T_{\text{eff}}=5961 \pm 27$ K, a surface gravity $\log g=4.5 \pm 0.1$, a metallicity $[\text{Fe}/\text{H}]=-0.01 \pm 0.04$ and a stellar mass $M_* = 1.17 \pm 0.12 M_\odot$.

From the SOPHIE CCF (Boisse et al. 2010b), we estimated $v \sin i_* = 3.7 \pm 1.0 \text{ km s}^{-1}$ and a metallicity of $[\text{Fe}/\text{H}]=0.08 \pm 0.10$ in agreement with the spectroscopic analysis. We estimate the stellar activity level from the emission in the core of the Ca II H&K bands measured on each SOPHIE spectra of HD150706 with the calibration reported in Boisse et al. (2010b). It yields a value of $\log R'_{\text{HK}}=-4.47 \pm 0.10$. HD150706 is an active star and we may expect a RV jitter due to stellar spots of about 15 ms^{-1} (Santos et al. 2000). According to the calibrations by Noyes et al. (1984) and Mamajek & Hillenbrand (2008), the $\log R'_{\text{HK}}$ value of HD 150706 implies a rotation period $P_{\text{rot}} \approx 5.6$ days. From the $v \sin i_*$ and stellar radius values, we can infer that $P_{\text{rot}} \leq 18$ days (Bouchy et al. 2005).

Holmberg et al. (2009) estimated an age of $5.1^{+3.7}_{-4.5}$ Gyr, in agreement with Marsakov et al. (1995) value of 4.69 Gyr. But younger ages were derived from Ca II measurements: 1.4 Gyr (Wright et al. 2004) and 1.16 Gyr (Rocha-Pinto et al. 2004), or from stellar isochrone: 2.3 Gyr (Gonzalez et al. 2010).

Meyer et al. (2004) detected a dust debris disk surrounding HD150706 thanks to IRAC and MIPS *Spitzer* instruments. The authors argued for the presence of a companion in order to explain their observation of a large inner hole in the dust distribution of the disk.

The parameter values for the star are collected in Table 2.

3.2. HD 222155

HD 222155 (HIP116616) is a G2V bright star with an apparent Johnson V-band magnitude of $m_V=7.1$ (Hipparcos catalogue, ESA 1997) and a $B-V=0.64$. Van Leeuwen (2007) derived from the Hipparcos measurements a parallax of 20.38 ± 0.62 mas, leading to infer a distance of 49.1 ± 1.5 pc with an absolute V magnitude of 3.65 mag.

The star's effective temperature $T_{\text{eff}} = 5765 \pm 22$ K, surface gravity $\log g = 4.10 \pm 0.13$, micro-turbulence velocity $V_t = 1.22 \pm 0.02 \text{ km s}^{-1}$, and metallicity $[\text{Fe}/\text{H}] = -0.11 \pm 0.05$ dex, was determined using the spectroscopic analysis method described in Santos et al. (2004). The analysis was performed on a high-SNR spectrum measured with SOPHIE without

a simultaneous calibration. When combined with isochrones (da Silva et al. 2006)¹, these parameters yield a stellar mass $M_* = 1.06 \pm 0.10 M_\odot$, a stellar radius of $R_* = 1.67 \pm 0.07 R_\odot$ and an age 8.2 ± 0.7 Gyr in agreement with 8.4 Gyr estimated by Holmberg et al. (2009). The value of the radius and the mass are in agreement with those derived by Allende-Prieto & Lambert (1999), $M_* = 1.20 \pm 0.11 M_\odot$ and $R_* = 1.66 \pm 0.07 R_\odot$. We chose for the stellar mass the mean value $M_* = 1.13 \pm 0.11 M_\odot$.

The projected rotational velocity $v \sin i_* = 3.2 \pm 1.0 \text{ km s}^{-1}$ is estimated from the SOPHIE CCF (Boisse et al. 2010b). The alternative estimation of the stellar metallicity $[\text{Fe}/\text{H}] = 0.02 \pm 0.10$ from the CCF is consistent with the more accurate determination based on spectral analysis. The stellar activity index is derived from the stellar spectra calculated in the Ca II H&K lines, $\log R'_{\text{HK}} = -5.06 \pm 0.10$. HD222155 is on its way to be a subgiant. These stars have a lower $\log R'_{\text{HK}}$ (Wright et al. 2004, Lovis et al. 2011b) due to their higher luminosities and/or lower surface gravities compared to main-sequence stars of the same color. These stars are expected to have less long-term variability than main-sequence stars. HD222155 is then a low-active star for which we expect intrinsic variability at a lower level than the instrumental effect. For $\log R'_{\text{HK}} \leq -5.0$, Mamajek & Hillenbrand (2008) noted that the correlation between $\log R'_{\text{HK}}$ and the Rossby number is poor that could not allow to derive a reliable P_{rot} .

The stellar parameters are given in Table 2.

4. RV analysis and planetary parameters

4.1. HD150706b, a Jupiter analogue around an active star

A Jupiter-mass planet in an eccentric 265-day orbit, HD150706b, was announced during the "Scientific Frontiers in Research on Extrasolar Planets" conference, Washington, in June 2002 from ELODIE RV measurements. But, new observations led to conclude that the RV variations are rather owing to a longer-period planet (S. Udry, private communication).

Using Eq. A.2 from the Appendix A, we first fixed the $\Delta(\text{RV})_{E-S}$ between ELODIE and SOPHIE data and computed the weighted and the generalized Lomb Scargle periodograms. For both, the highest peak is detected close to 5000 days with false alarm probability (fap) <0.001 . The fap was generated using both Monte-Carlo simulations to draw new measurements according to their error bars and random permutation of the date of the observations, as described in Lovis et al. (2011a).

Eight Keck measurements were published by Moro-Martín et al. (2007). We add these measurements to our RV data. An error of 5 ms^{-1} were quadratically added to their instrumental error bars in order to take into account the stellar activity jitter. The RV were then fitted with a Keplerian model using a Levenberg-Marquardt algorithm, after selecting starting values with a genetic algorithm (Ségransan et al. 2011). The $\Delta(\text{RV})_{E-S}$ was allowed to vary and the fitted value, $-31.1 \pm 13.6 \text{ ms}^{-1}$ is in agreement with the calibration $\Delta(\text{RV})_{E-S} = -40 \pm 23 \text{ ms}^{-1}$. The best solution is consistent with an orbital period of $P=3950$ days and a semi-amplitude $K=31 \text{ ms}^{-1}$. The residuals to the best-fit Keplerian model are equal to $\sigma_{(O-C)}=19.5 \text{ ms}^{-1}$, that divide out in 18 ms^{-1} for the ELODIE RV, 6.1 ms^{-1} for the Keck and 20 ms^{-1} for the SOPHIE ones. These values are large compared to the mean error bars.

HD150706 is an active star and we may expect some RV jitter as discussed in Sect. 3.1. We note that looking at the peri-

¹ Web interface available on <http://stev.oapd.inaf.it/cgi-bin/param>.

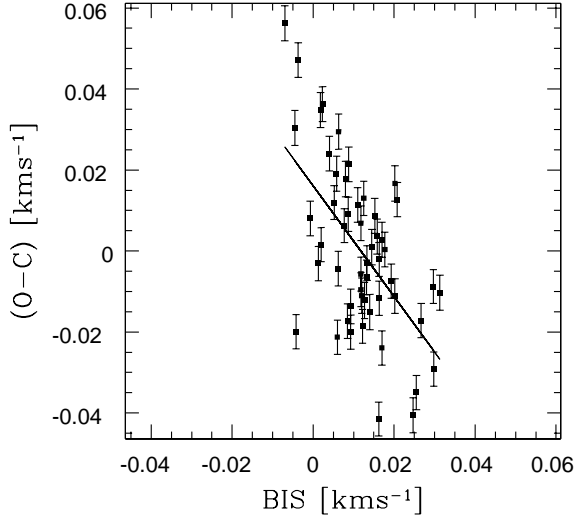


Fig. 1. SOPHIE residuals from the Keplerian fit of HD150706 as a function of the BIS. The best-linear fit is plotted as a black line. The scale is the same in the x and y axis.

odogram of the $(O - C)$, a peak close to 10 days is scarcely detected, value in the domain of the P_{tot} that we derive in Sect.3.1. With a $v \sin i = 3.7 \text{ km s}^{-1}$, an anti-correlation between the $(O - C)$ and the bisector span (BIS) is expected if RV variations are due to stellar activity. The ELODIE measurements have an error bars of about 10 ms^{-1} for the RV and 20 ms^{-1} for the BIS. This precision hampers the detection of a correlation for data with a dispersion of 16 ms^{-1} . On the other hand, an anti-correlation is observed in the SOPHIE data as shown in Fig. 2. The correlation coefficient is equal to -0.56 with a $\text{fap} < 10^{-5}$ and the Spearman coefficient is of -0.47 . The fap is calculated with random permutations of the RV data. As in Melo et al. (2007) and in Boisse et al. (2009), we corrected the SOPHIE RV from this trend $RV_{corrected1} [\text{km s}^{-1}] = RV [\text{km s}^{-1}] + 1.32 \times BIS [\text{km s}^{-1}]$.

Moreover, at high SNR, SOPHIE data are polluted by an instrumental limitation, called *seeing effect* (Boisse et al. 2010a,b). This apparent RV shift is related to the illumination of the spectrograph that varies mainly with the seeing. Its current characteristic signature is a linear correlation between the RV and a *seeing estimator* Σ accounting for the flux entrance in the spectrograph per unit of time, $\Sigma = SNR^2 / T_{\text{exp}}$, with T_{exp} the time exposure. The HD150706 SOPHIE $(O - C)$ are plotted in Fig. 2. A linear trend is detected with a correlation and a Spearman coefficients of -0.48 with $\text{fap} < 10^{-4}$. The SOPHIE RV was corrected from this slope: $RV_{corrected2} [\text{km s}^{-1}] = RV_{corrected1} [\text{km s}^{-1}] + 0.00071 \times \Sigma$. We note that to swap the order of the corrections do not change the final result as the order of magnitude of the two effects are equivalent.

At last, we fitted using a Keplerian model the ELODIE and Keck measurements together with the corrected SOPHIE ones. The final orbital elements are listed in Table 3. They are computed from $4.8 \cdot 10^6$ Monte Carlo simulations with a prior on the $\Delta(RV)_{E-S}$ equals to the calibrated value and its uncertainty. The uncertainties of the final parameters correspond to the 0.95 confidence interval. The best solution is consistent with a non-significant eccentric orbit, $e = 0.38^{+0.28}_{-0.32}$, with a period of $P = 5894^{+5584}_{-1498}$ days and a semi-amplitude $K = 31.1^{+6.3}_{-4.8} \text{ ms}^{-1}$. Taking into account the error bar on the stellar mass, HD150706b is a planet with a minimum mass $m_p \sin i = 2.71^{+1.14}_{-0.66} M_{Jup}$ orbiting its star with a semi-major axis

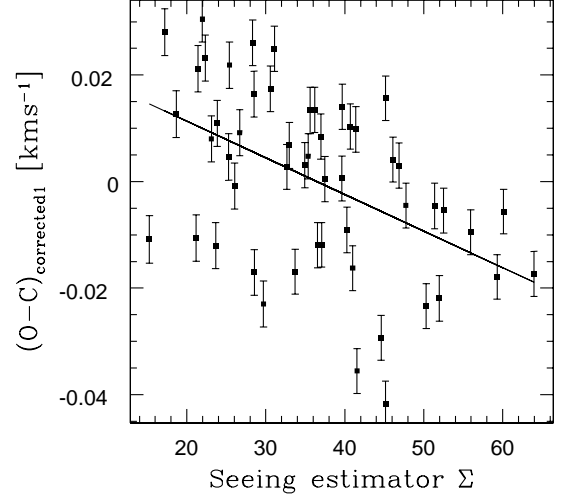


Fig. 2. HD150706 SOPHIE residuals from the Keplerian fit of the RV corrected from the active jitter as a function of the *seeing estimator*, illustrating the instrumental effect on RV due to seeing variations. The best-least-square linear fit is also plotted.

of $6.7^{+4.0}_{-1.4}$ AU. In Fig. 3, the best-fit Keplerian model is superimposed to the ELODIE, Keck and SOPHIE velocities. We also add plots in Fig.4 to illustrate the dependence of the K, P and e parameters with $\Delta(RV)_{E-S}$.

We did not find any indication for a second planet in the system with the current data set. From our solution, with a dispersion of 15 ms^{-1} , the RV residuals exclude an inner planet with $m_p \sin i > 1.3 M_{Jup}$. On the other hand, during the time span of 13.3 yr of our observations, we should not have missed an external planet that induces a drift larger than $1.1 \text{ ms}^{-1} \text{ yr}^{-1}$.

Table 3. Keplerian solution and inferred planetary parameters for HD150706b and HD222155b (see text for details).

Parameters	HD150706b	HD222155b
RV_{mean} ELODIE [km s^{-1}]	$-17.2094^{+0.0145}_{-0.0064}$	$-43.9923^{+0.0042}_{-0.0052}$
RV_{mean} SOPHIE [km s^{-1}]	$-17.1271^{+0.0127}_{-0.0118}$	$-43.9007^{+0.0129}_{-0.0114}$
RV_{mean} KECK [km s^{-1}]	$0.0322^{+0.0074}_{-0.0075}$	
P [days]	5894^{+5584}_{-1498}	3999^{+469}_{-541}
K [m s^{-1}]	$31.1^{+6.3}_{-4.8}$	$24.2^{+6.4}_{-4.8}$
e	$0.38^{+0.28}_{-0.32}$	$0.16^{+0.27}_{-0.22}$
ω [deg]	132^{+37}_{-33}	137^{+240}_{-52}
T_0 [JD]	58179^{+4396}_{-1586}	56319^{+664}_{-498}
$m_p \sin i$ [M_{Jup}]	$2.71^{+1.14}_{-0.66} *$	$1.90^{+0.67}_{-0.53} *$
a [AU]	$6.7^{+4.0}_{-1.4} *$	$5.1^{+0.6}_{-0.7} *$
$\sigma_{(O-C)}$ ELODIE [m s^{-1}]	15.3	11.5
$\sigma_{(O-C)}$ SOPHIE [m s^{-1}]	14.2	9.9
$\sigma_{(O-C)}$ KECK [m s^{-1}]	6.2	

* assuming $M_* = 1.17 \pm 0.12 M_{\odot}$

* assuming $M_* = 1.13 \pm 0.11 M_{\odot}$

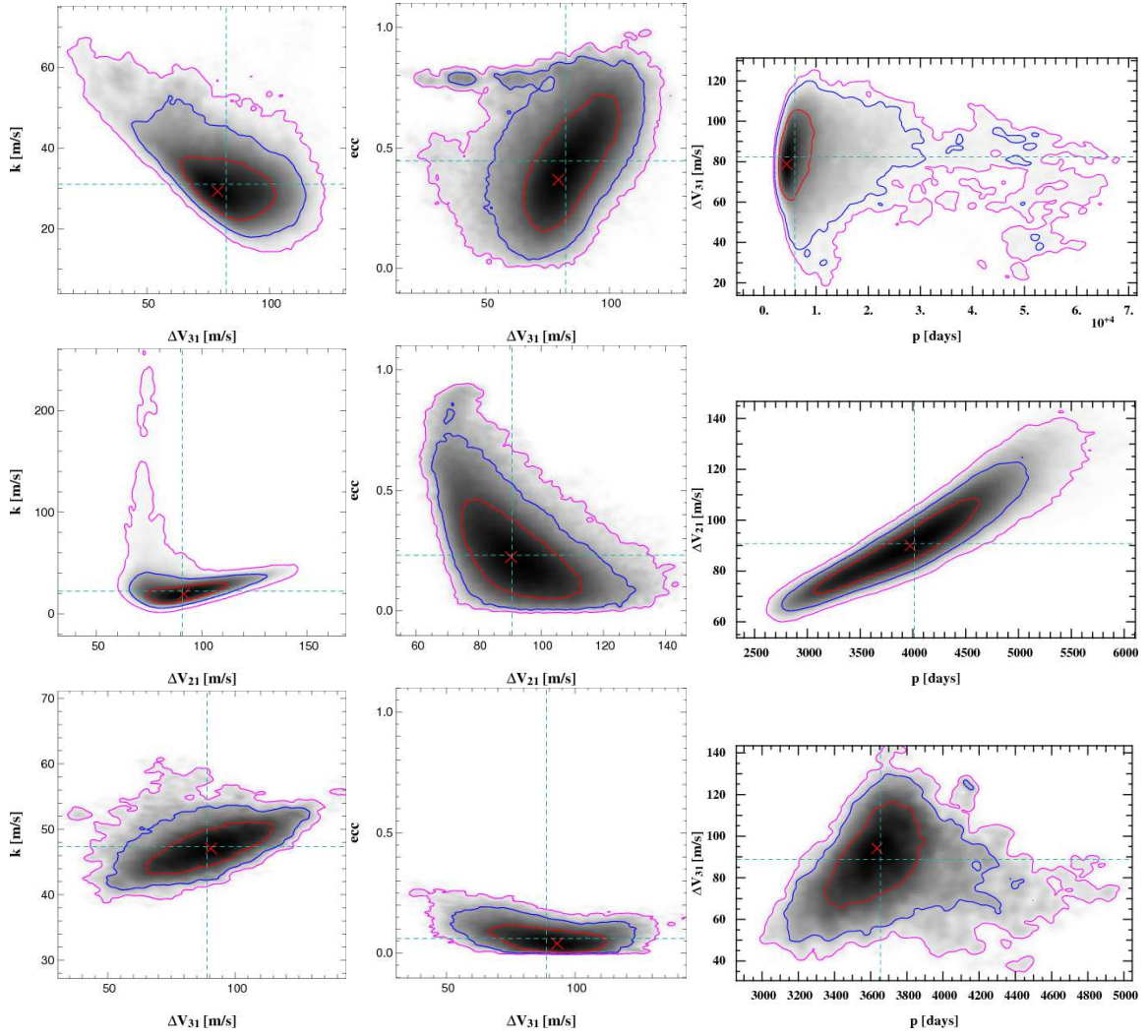


Fig. 4. Covariance between the semi-amplitude K (left panels), the eccentricity e (middle panels), the period P (right panels) and the $\Delta(\text{RV})_{E-S}$ for the HD150706 (top panels), HD222155 (middle panels) and HD24040 systems (bottom panels). The red, blue and purple contour lines represent respectively the one, two and three- σ confidence intervals.

4.2. HD222155b, a Jupiter analogue around a quiet star

We used the same methodology as for HD150706. First, we fixed the $\Delta(\text{RV})_{E-S}$ thanks to the calibration (Appendix A) and used Lomb Scargle periodogram to estimate the significance level of the detection of a long-period planet. With a $\text{fap} < 0.001$, the highest peak corresponds to a period close to 4000 days.

The ELODIE and SOPHIE RV were then fitted with a Keplerian model. The eccentricity was set as a free parameter, as well as the RV offset between the data sets. The fitted offset $-49 \pm 8 \text{ m s}^{-1}$ is in agreement with the calibrated one within the error bars, $-70 \pm 23 \text{ m s}^{-1}$. The orbit has a non significant eccentricity with $e = 0.26 \pm 0.24$, a semi-amplitude $K = 20.1 \text{ m s}^{-1}$ and a period of 3259 days. The residuals to the fit $\sigma_{(O-C)} = 19.9 \text{ m s}^{-1}$ are large compared to the mean error bar.

The star is inactive and we do not expect any jitter as an astrophysical noise. On the other hand, the *seeing effect* is characterized in the SOPHIE data. In Fig. 5, SOPHIE residuals are plotted as a function of the *seeing estimator* Σ . The correlation coefficient is equal to -0.51 and the Spearman coefficient to -0.5 with $\text{fap} < 10^{-5}$, justifying a linear least-square fit to the data. We corrected the SOPHIE RV from this trend $RV_{\text{corrected}} [\text{kms}^{-1}] = RV [\text{kms}^{-1}] + 0.00068 \times \Sigma$.

We then fitted with a Keplerian model the corrected SOPHIE RV and the ELODIE measurements. The final orbital elements are computed from $4.8 \cdot 10^6$ Monte Carlo simulations with a prior on the $\Delta(\text{RV})_{E-S}$ equals to the calibrated value and its uncertainty (and accounting for the correction on the SOPHIE RV). The uncertainties correspond to the 0.95 confidence interval. They are listed in Table 3. The best solution is a non-significant eccentric orbit ($e = 0.16^{+0.27}_{-0.22}$) with a period $P = 3999^{+469}_{-541}$ days and a semi-amplitude $K = 24.2^{+6.4}_{-4.8} \text{ m s}^{-1}$. The corresponding planet has a minimum mass of $m_p \sin i = 1.90^{+0.67}_{-0.53} M_{Jup}$ and orbits HD222155 with a semi-major axis of $5.1^{+0.6}_{-0.7} \text{ AU}$ taking into account the error bar on the stellar mass. In Fig. 6, the best-fit Keplerian model is superimposed to the ELODIE and SOPHIE velocities. Plots in Fig. 4 show the covariance of the K , P and e parameters with $\Delta(\text{RV})_{E-S}$.

No periodicity is detected in the RV residuals. The dispersion of the residuals, $\sigma_{(O-C)} \sim 11 \text{ m s}^{-1}$, excludes an inner planet with $m_p \sin i > 0.9 M_{Jup}$ and an external planet should not induce a drift larger than $0.8 \text{ m s}^{-1} \text{ yr}^{-1}$.

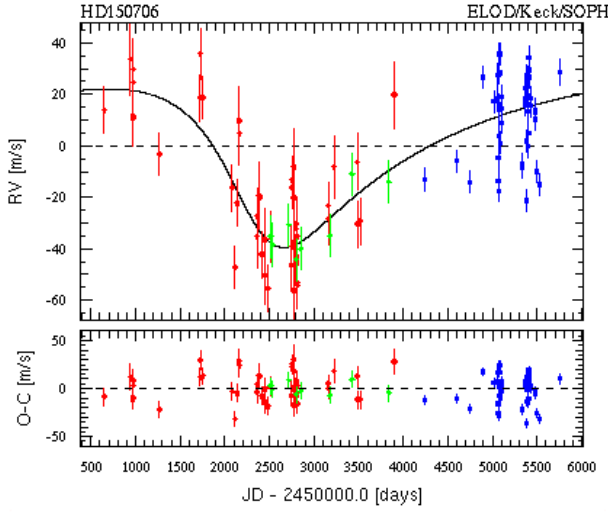


Fig. 3. ELODIE (red), Keck (green) and SOPHIE (blue) RV and residuals to the best-fit Keplerian model for HD150706 as a function of barycentric Julian date. The best-fit Keplerian model is represented by the black curve with a reduced χ^2 equal to 2.6. The period is 16.1 yr with a slight eccentricity $e=0.38^{+0.28}_{-0.32}$ and the planet minimum mass is $2.71 M_{Jup}$.

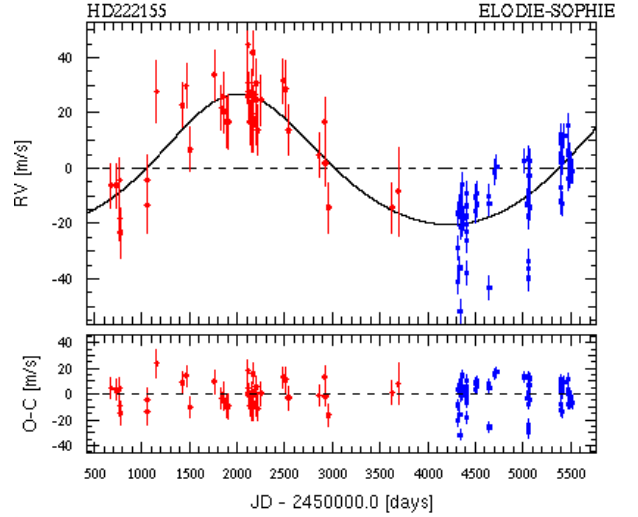


Fig. 6. ELODIE (red) and SOPHIE (blue) RV and residuals to the best-fit Keplerian model for HD222155 as a function of barycentric Julian date. The best-fit Keplerian model is represented by the black curve with a reduced χ^2 equal to 2.2. The planet has a period of 10.9 yr in a non-significant eccentric orbit ($e=0.16^{+0.27}_{-0.22}$), and a minimum mass of $1.90 M_{Jup}$.

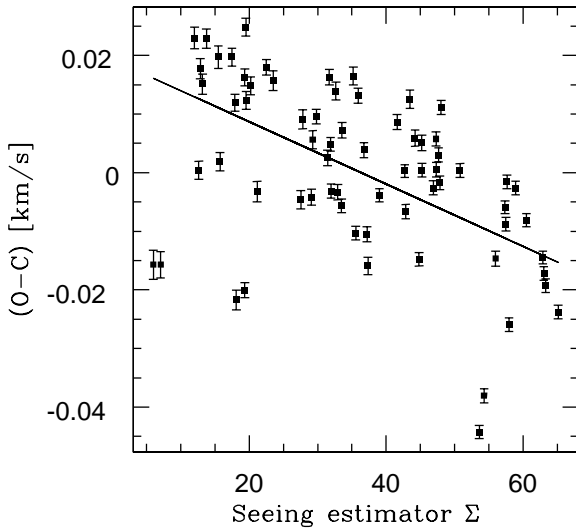


Fig. 5. SOPHIE residuals from the Keplerian fit of HD222155 as a function of the *seeing estimator*. The best-least-square linear fit is also plotted.

5. Refine long-period announced planets

The following targets were measured for the same subprogram and observed with the same strategy than for HD150706 and HD222155 as detailed in Sect. 2.

5.1. HD24040b

Wright et al. (2007) presented HD24040b from the RV variability measured on the inactive G0V star with the Keck. At that time, the authors announced a companion with a period between 10 and 100 years and a minimum mass in the range between 5 and $20 M_{Jup}$. The stellar parameters can be found in Table 2 of Wright et al. (2007).

Our observations of HD24040, obtained over, respectively, September 1997 and December 2005, and February 2008 and December 2010, have provided 47 ELODIE and 20 SOPHIE measurements. The SOPHIE data with $SNR < 100$ were removed (four observations) and three measurements with abnormal flux of the calibrating thorium-argon lamp were discarded.

We combined the ELODIE and SOPHIE datasets (available electronically in Tables A.5 and A.6) with the published Keck ones to derive planetary parameters. The best Keplerian fit converges with a RV offset between ELODIE and SOPHIE of $\Delta(RV)_{E-S} = -120 \pm 12 \text{ ms}^{-1}$ significantly higher than the calibrated value $-74 \pm 23 \text{ ms}^{-1}$ for this star with a $B - V = 0.64$. Moreover, the RV show a trend as seen in Fig. 8. We then fit the RV measurements with a Keplerian and a linear trend. We search for the *seeing effect* in the residuals of the fit. The SOPHIE ($O-C$) are plotted as a function of the *seeing estimator* in Fig. 7. The correlation coefficient, equals to -0.30 , is not significant with 30% probability that the two variables are uncorrelated. We removed from the study the measurement with the highest *seeing estimator* value, certainly biased by the *seeing effect*.

We re-adjust the data with a simultaneous fit of a Keplerian and a linear trend. The RV offset is equal to $-67 \pm 13 \text{ ms}^{-1}$ in agreement within the error bars with the calibrated value. The final orbital elements are computed from $4.8 \cdot 10^6$ Monte Carlo simulations with a prior on the $\Delta(RV)_{E-S}$ equals to the calibrated value and its uncertainty. Fig. 8 shows the velocities as a function of time, as well as the fitted Keplerian orbit with a period of 3668 days and the linear trend of $3.85^{+1.43}_{-1.29} \text{ ms}^{-1} \text{ yr}^{-1}$. The underlying linear drift easily explains why Wright et al. (2007) overestimated the period and the mass of HD24040b when fitting over a fraction of the orbital period. The solution is circular, $e=0.04^{+0.07}_{-0.06}$, with a semi-amplitude of $K=47.4^{+2.7}_{-2.6} \text{ ms}^{-1}$. The inferred minimum mass of the companion, accounting for the uncertainty on the stellar mass, is $4.01 \pm 0.49 M_{Jup}$ with a semi-major axis of $4.92 \pm 0.38 \text{ AU}$ (Table 5). The dependencies of the K, P and e parameters and of the linear trend with $\Delta(RV)_{E-S}$ is plotted in Fig. 4.

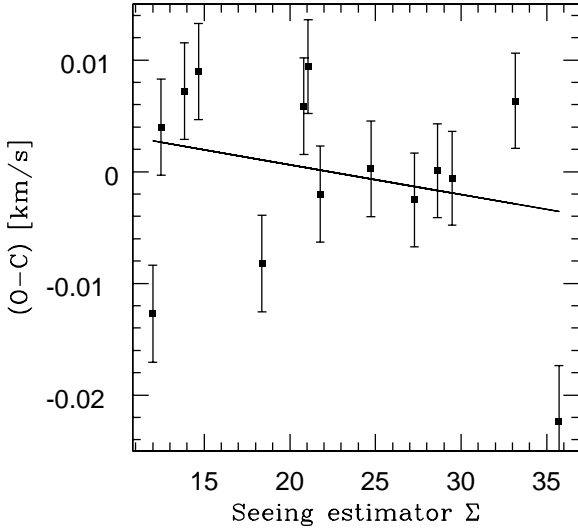


Fig. 7. HD24040 SOPHIE residuals from the Keplerian fit as a function of the *seeing estimator*. The linear trend is not significant.

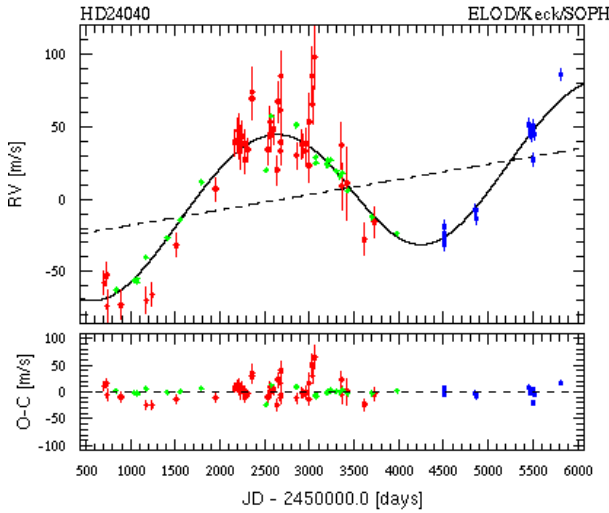


Fig. 8. ELODIE (red), Keck (green) SOPHIE (blue) RV and residuals to the best-fit Keplerian model (black curve) for HD24040 as a function of barycentric Julian date. It shows a $4.92 M_{Jup}$ companion with an orbital period of 10.0 yr. A linear trend is fitted simultaneously pointing out the presence of a third body in the system.

With a dispersion of 7.5 ms^{-1} , the residuals do not show evidence for shorter period companion, and an inner planet with $m_p \sin i > 0.62 M_{Jup}$ is excluded.

5.2. HD89307b

Observed from the Lick Observatory since 1998, Fischer et al. (2009) published a companion of $m_p \sin i = 1.78 \pm 0.13 M_{Jup}$ with a period of 2157 ± 63 days and an eccentricity of 0.24 ± 0.07 in orbit around HD89307, a bright inactive G0 dwarf. We refer the reader to the Fischer et al. (2009) stellar parameters (cf. their Table 1). We note that their stellar values are in agreement with those derived by Sousa et al. (2006) from SARG observation at TNG.

Table 5. Keplerian solution and inferred planetary parameters for HD24040b with the combined measurements of ELODIE, SOPHIE and the Keck RV data published by Wright et al. (2007).

Parameters	HD24040b
RV_{mean} ELODIE [km s^{-1}]	-9.4003 ± 0.0040
RV_{mean} SOPHIE [km s^{-1}]	$-9.3118^{+0.0150}_{-0.0156}$
RV_{mean} KECK [km s^{-1}]	$0.0311^{+0.0039}_{-0.0036}$
RV_{linear} [$\text{m s}^{-1}\text{yr}^{-1}$]	$3.85^{+1.43}_{-1.29}$
P [days]	3668^{+169}_{-171}
K [m s^{-1}]	$47.4^{+2.7}_{-2.6}$
e	$0.04^{+0.07}_{-0.06}$
ω [deg]	154^{+84}_{-54}
T_0 [JD]	54308^{+859}_{-839}
$m_p \sin i$ [M_{Jup}]	4.01 ± 0.49^1
a [AU]	4.92 ± 0.38^1
$\sigma_{(O-C)}$ ELODIE [m s^{-1}]	14.9
$\sigma_{(O-C)}$ SOPHIE [m s^{-1}]	7.3
$\sigma_{(O-C)}$ KECK [m s^{-1}]	7.2

¹ assuming $M_\star = 1.18 \pm 0.10 M_\odot$

We have 46 ELODIE and 11 SOPHIE measurements obtained respectively between December 1997 and April 2006, and between December 2006 and February 2011. They are available electronically in Tables A.7 and A.8. We combined our measurements with the Lick RV. Figure 9 shows the Keplerian orbit and the residuals around the solution. The RV shift between ELODIE and SOPHIE, $\Delta(RV)_{E-S} = -66 \pm 12 \text{ ms}^{-1}$, is in agreement with the calibrated one, $-49 \pm 23 \text{ ms}^{-1}$. No instrumental effect is observed in the SOPHIE data. The planetary parameters are in agreement with Fischer et al. (2009). The fitted parameters for the companion and their uncertainties computed from 5000 permutations simulations and the 0.95 confidence interval are listed in Table 9. Assuming a stellar mass of $M_\star = 1.03 M_\odot$ and taking into account its uncertainty ($\pm 0.10 M_\odot$), we compute a planetary minimum mass of $m_p \sin i = 2.0 \pm 0.4 M_{Jup}$ for the HD24040 companion, slightly higher than the previous published value. The planet has a little higher period of 2199 ± 61 days and orbits at 3.34 ± 0.17 AU. We confirm the probable eccentricity orbit with $e = 0.25 \pm 0.09$.

The residuals do not show periodicity. With a dispersion of 8 ms^{-1} , the residuals do not permit the presence of an inner planet with a minimum mass $m_p \sin i > 0.5 M_{Jup}$.

5.3. HD154345b

Wright et al. (2008) reported the detection of HD154345b with a minimum mass of $m_p \sin i = 0.94 \pm 0.09 M_{Jup}$, an orbital period $P = 3539 \pm 66$ d, and a non-significant eccentricity of $e = 0.044 \pm 0.046$. The host star is a bright quiet G8V ($m_V = 6.7$) with an estimated mass $M_\star = 0.88 \pm 0.09 M_\odot$. The stellar parameters can be found in the Table 1 of Wright et al. (2008).

The star was also observed by ELODIE and SOPHIE with respectively 49 and 15 measurements spanning 12.2 and 3.2 yr. Three measurements were removed in the SOPHIE sample owing to abnormal flux of the thorium-argon calibration lamp and one due to too low SNR. We combined these measurements (available electronically in Tables A.9 and A.10) with

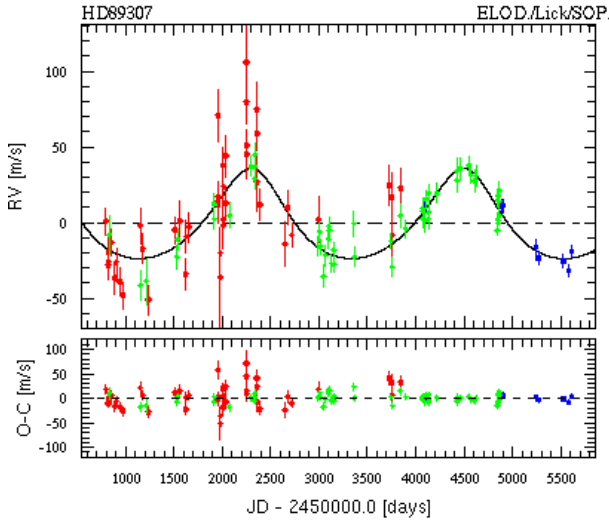


Fig. 9. ELODIE (blue), Lick (green) and SOPHIE (red) RV and residuals to the best-fit Keplerian model (black curve) for HD89307 as a function of time. The fitted orbit corresponds to a planet with a minimum mass of $2.0 M_{Jup}$, a period of 6.0 yr, and a slightly eccentricity orbit $e=0.25\pm 0.09$.

the Keck RV and fit them with a Keplerian model. The best fit converges with a RV offset between ELODIE and SOPHIE of $\Delta(RV)_{E-S}=107\pm 6\text{ms}^{-1}$, in agreement with the calibrated one of $108\pm 23\text{ms}^{-1}$ for this star with a $B - V=0.73$ (see App. A). We searched for the *seeing effect* in the SOPHIE data. As in HD24040, we found only one measurements significantly affected by the instrumental effect (at BJD=54261). We removed it from the sample and fit the three data sets with a Keplerian model. We found the best solution with equivalent mass and period than Wright et al. (2008) and a non-significant eccentricity $e=0.26\pm 0.15$. The fitted parameters for the companions and their uncertainties computed from 5000 permutations simulations and the 0.95 confidence interval are listed in Table 9. The final RV offset is equal to $\Delta(RV)_{E-S}=112\pm 10\text{ms}^{-1}$. We infer a minimum mass of $1.0\pm 0.3 M_{Jup}$, and semi-major axis of 4.3 ± 0.4 AU. The error bars take into account the uncertainty on the stellar mass. The best-fit is plotted in Fig. 10. No significant variability is found in the residuals, and with a total dispersion of 4ms^{-1} , inner planet with $m_p \sin i > 0.3 M_{Jup}$ is not allowed.

6. Are we observing magnetic cycles ?

Planet discoveries with orbital periods reaching the range where stellar magnetic cycles have been observed (from 2.5 to 25 years, Baliunas et al. 1995) are recent. A magnetic cycle could induce RV variations with the periodic modification of the number of spots and plages on the stellar photosphere (as we observed on the Sun on a 11-year period), related to change in the convection pattern and/or other mechanisms like meridional flows (Beckers 2007, Makarov 2010), owing to the magnetic field created by dynamo. The $\log R'_{HK}$ index, computed from the Ca II H&K lines is sensitive to the presence of plages in the stellar chromosphere and is a good indicator to monitor the magnetic cycle.

Dedicated observations of stars with known magnetic cycles in RV (Santos et al. 2010a, Gomes da Silva et al. 2011) observed faint correlations between index in active lines (Ca II H&K, H α , Na I) and RV, as well as in the parameters of the CCF. But these

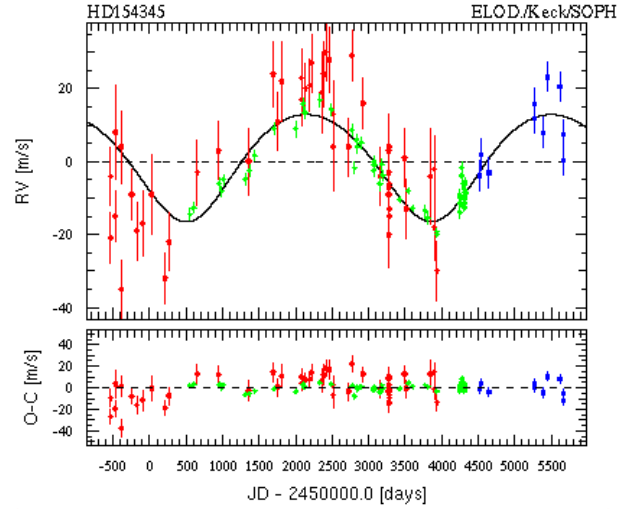


Fig. 10. ELODIE (red), Keck (green) and SOPHIE (blue) RV and residuals to the best-fit Keplerian model (black curve) for HD154345 as a function of barycentric Julian date. The companion has a period of 9.7 yr, and a minimum mass of $1.0 M_{Jup}$.

Table 9. Keplerian solution and inferred planetary parameters for HD154345b and HD89307b with the combined measurements of ELODIE, SOPHIE and the already published RV data.

Parameters	HD154345b	HD89307b
RV_{mean} ELODIE [km s $^{-1}$]	-46.954 ± 0.005	23.067 ± 0.005
RV_{mean} SOPHIE [km s $^{-1}$]	-46.842 ± 0.005	23.133 ± 0.007
RV_{mean} ORIGINAL RV [km s $^{-1}$]	-0.004 ± 0.005^A	0.007 ± 0.005^B
P [days]	3538 ± 300	2199 ± 61
K [m s $^{-1}$]	17.0 ± 3.7	32.4 ± 4.5
e	0.26 ± 0.15	0.25 ± 0.09
ω [deg]	-14 ± 160	14 ± 33
T_0 [JD]	54701 ± 1000	54549 ± 190
$m_p \sin i$ [M_{Jup}]	1.0 ± 0.3^1	2.0 ± 0.4^2
a [AU]	4.3 ± 0.4^1	3.34 ± 0.17^2
$\sigma_{(O-C)}$ ELODIE [m s $^{-1}$]	12.9	19.5
$\sigma_{(O-C)}$ SOPHIE [m s $^{-1}$]	6.6	4.1
$\sigma_{(O-C)}$ ORIGINAL RV [m s $^{-1}$]	2.9 ^A	8.4 ^B

^A Keck RV (Wright et al. 2008)

^B Lick RV (Fischer et al. 2009)

¹ assuming $M_\star = 0.88 \pm 0.09 M_\odot$

² assuming $M_\star = 1.03 \pm 0.10 M_\odot$

studies were limited on a short range of spectral type, respectively early-K and early-M dwarfs.

On the other hand, high-precision stabilized fiber-fed spectrographs that observe in the visible like HARPS or SOPHIE can measure accurately the flux in the Ca II H&K lines. They can monitor with high-precision the variation with time of the $\log R'_{HK}$ index (Lovis et al. 2011b). While searching for planets, HARPS RV measurements reveal stellar magnetic cycles (Moutou et al. 2011, Ségransan et al. 2011, Dumusque et al. 2011). Lovis et al. (2011b) used the HARPS sample to identify activity cycles and to derive relations of the RV and the CCF parameters variations as a function of the R'_{HK} variability. These relations depend on the stellar effective temperature and could be used to estimate the RV jitter produced by a magnetic cycle.

The FWHM or contrast of the CCF are not sufficiently accurate on ELODIE or SOPHIE measurements to examine their

variations. As well, the accuracy on the ELODIE BIS is too low to be sensitive to the effect of a magnetic cycle. Moreover, the use of the thorium-argon lamp during the observations yields polluted light on the CCD detector that prevent the measurement of the flux inside the active lines for ELODIE spectra. Only SOPHIE measurements of active lines can be used on a shorter timescale (~ 3 years) to check for a stellar variability. Our observations alone can not conclude about the existence of magnetic cycles on the reported stars. Pursuing the observations is then needed.

Nevertheless, we measured the Pearson and Spearman correlation coefficients between the $\log R'_{HK}$ and the RV values extracted from the SOPHIE data. For the only active star of the sample, HD150706, we average the measurements by bin of 30 days in order to remove the effect of the rotational period. We tested the significance of these coefficients with 100,000 MonteCarlo simulations of shuffled data. We did not find any correlation that could put in doubt the planetary hypothesis.

We can come to an assessment using the Lovis et al. (2011b) work and relations. We observed in their Fig. 19 that the maximal RV amplitude induced by a magnetic cycle is 12 ms^{-1} . The detected RV semi-amplitude reported in our paper are all greater than 17 ms^{-1} , the smaller one being for HD154345. Using the Eq. 9 from Lovis et al. (2011b) and the calcium index variations published by Wright et al. (2008), we calculated that the expected RV semi-amplitude due to an active cycle for HD154345 is $3.65 \pm 0.41 \text{ ms}^{-1}$, far below the observed one. As another example, the $\log R'_{HK}$ semi-amplitude needed to induce the RV variation measured on HD89307 is two times higher than the highest modulation observed by Lovis et al. (2011b) due to magnetic cycle (cf. their Fig. 10). We concluded that the best possible explanation to the observed RV variations for our stars are the planetary hypothesis.

7. Concluding remarks

We announce the detection of two new Jupiter-like planet candidates around HD150706 and HD222155 with combined measurements from the ELODIE and the SOPHIE spectrographs, successively mounted on the 1.93-m telescope at the OHP. Orbiting farther than 5 AU from their stars, the planets have minimum masses of respectively, 2.71 and $1.90 M_{Jup}$. We also published the first reliable orbit for HD24040b, another gaseous long-period planet. We determined a minimum mass of $4.01 M_{Jup}$ for this planet in a 10.0 yr orbit at 4.92 AU. We also present evidence for a third companion in this system. Moreover, we refine the planetary parameters of two others Jupiter-analogues, HD154345b and HD89307b, combining our RV with, respectively, the Keck and the Lick observatories measurements. We obtain parameter values in agreement with Wright et al. (2008) and Fischer et al. (2009).

HD150706 is an active star and the signature of its effect is detected in the BIS of the CCF. We corrected the SOPHIE measurements from the jitter effect. The four others stars are quiet with $\log R'_{HK}$ values lower than -4.9 . On the contrary, the SOPHIE measurements showed an instrumental effect related to seeing variations that we partly corrected.

The amplitudes of the RV variations are greater for all stars than for all the reported active cycles in the literature (Baliunas et al. 1995, Lovis et al. 2011b). We did not find any long-term correlations between the RV and the activity index on the SOPHIE measurements. We concluded that the best explanation

for the observed RV variations are the planetary hypothesis.

Meyer et al. (2004) detected on HD150706, with IRAC and MIPS for *Spitzer*, an infrared excess at $70 \mu\text{m}$, an upper limit at $160 \mu\text{m}$ and no evidence for excess at $\lambda < 35 \mu\text{m}$. They interpreted their observations as a dust disk surrounding the star with a hole devoid of dust with an inner radius of at least 20 AU. The authors supposed the presence of an exoplanet to explain the inner edge of the outer dust disk. SOPHIE and ELODIE RV show evidence for a large companion at less than 20 AU around HD150706. With a minimum mass of $2.71 M_{Jup}$, HD150706b orbiting at $6.7_{-1.4}^{+4.0}$ AU could keep clear the inner region of the disk.

Looking at the current distribution of the periodicities of the exoplanet candidates discovered by RV (Fig. 11), we observe a drop after ≈ 4 AU. These long-period planets are part of a new parameter space detections, reached thanks to the extension of the RV surveys with databases of more than 15 years. The current paper increases to nineteen the number of planets further than 4 AU characterized from RV measurements (Table 1). With partial observations (orbital period not completely covered) and a small number of objects, it is difficult to converge on significant statistic trends.

Nevertheless, in Fig. 12, we zoom on the planets discovered beyond 4 AU. We remark that no very massive planets ($> 8 M_{Jup}$) is found beyond 4 AU, in spite of a RV bias detection toward high-mass objects. We emphasize that the only one, HD106270b, is a particular object reported by Johnson et al. (2011) as a very massive planet ($m_p \sin i = 11 M_{Jup}$) orbiting a subgiant. The occurrence rate of planets with minimum mass higher than $8 M_{Jup}$ is of $1/19$ for semi-major axes $a > 4$ AU compared to $27/196$ ($\approx 1/7$) for smaller orbits with $1 < a < 4 \text{ AU}^2$. **Considering binomial distribution, it leads that $13.8 \pm 2.5\%$ of the planets with semi-major axes in the range $1 < a < 4 \text{ AU}$ have a minimum mass higher than $8 M_{Jup}$ and $5.3 \pm 22.3\%$ for those with semi-major axes $a > 4 \text{ AU}$. The last error bar illustrates the small numbers statistic. It is unlikely that such host stars would have been discarded from planet surveys as being single-lined spectroscopic binaries (a $8 M_{Jup}$ orbiting in 4000 days a one solar-mass star induces a RV semi-amplitude of 102 ms^{-1} for a circular orbit, that leads to a typical linear slope of $\sim 37 \text{ ms}^{-1} \text{ yr}^{-1}$). If this result is not owing to an observational selection effect, and if we consider that these objects are formed by core-accretion, an explanation could be that these planets did not migrate a lot, preventing a high accumulation of material. Or else, the disk could dissipate at the time than the formation of these planets preventing them from migrating and growing in mass.**

If we consider only the planets published with a complete coverage of their orbits, they are mostly non-eccentric ($e < 0.25$). On the contrary, those with non-complete coverage are almost entirely eccentric ($e > 0.25$) reflecting that eccentric orbits are more easily detected for periods longer than observations times (Cumming 2004). However, the eccentricity distribution of these planets is in agreement with the current observation of a significant dispersion in eccentricities. But we emphasize that a slight eccentricity may hide a longer period planet.

We observe that these planets are rather found in multi-planetary systems (10 over 19 candidates). This could be due to an observational bias as systems with planets are preferentially followed-up. The multiple systems (including HD24040)

² Statistics done from the catalogue of the website *exoplanet.eu*

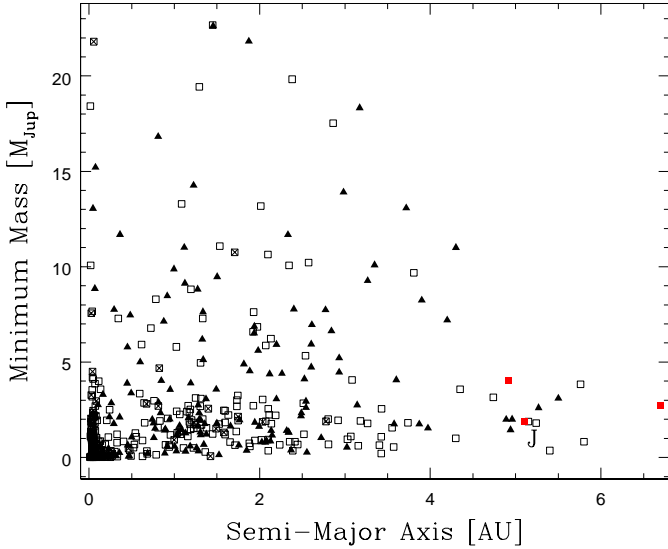


Fig. 11. Minimum mass as a function of the semi-major axis for all planets detected by RV and transit surveys. Empty squared (filled triangles) are for planets with eccentricity lower (higher) than 0.25. Crosses showed fixed eccentricity at $e=0$. Jupiter is on the plot. Red points are the Jupiter-like planets characterized in this paper: HD150706b, HD222155b, and HD24040b.

are plotted in Fig. 13. We remark the presence of two of the most populated systems, μ Ara (HD160691) and 55 Cnc (HD75732) with respectively, four and five planets. For them, the longer period planet is the higher mass one. HD134987 and HD183263 present the same configuration that our Jupiter-Saturne system with a lower mass planet outside. Two stars, HD187123 and HD217107, host also a short-period giant planet.

Most of the host-stars are G-type dwarf stars. It is clearly an observational bias, as G-type stars were the first spectral type measured by RV surveys. Fig. 14 shows the distribution of the metallicity of the host-stars. These detections come from different surveys and samples, and it is not easy to compare the occurrence rate. Nevertheless, a first observation should be that the distribution follows the property that giant gaseous planets are found significantly around more metal-rich stars than average (Santos et al. 2004, Fischer & Valenti 2005).

These giants planets are supposed to be formed beyond the "snow line". According to the models of planet formation and orbital evolution, giant planets migrate inward on a time scale that competes with the lifetime of the protoplanetary disk. These giants planets with long-orbital period should have not migrated or followed a scenario that bring them at this location. They may have formed as the same time as the disk dissipate preventing them from migration. They also may have interacted with other planets in the system that bring them to migrate outwards or hamper their migration. For example, avoid inward migration could be done by resonance trapping if the mass of the outer planet is a fraction of the mass of the inner planet, as in the Jupiter-Saturn case (Masset & Snellgrove, 2001, Morbidelli & Crida, 2007).

Bright ($6.7 < m_V < 7.6$) and nearby (between 18 and 49 pc), these targets are favorable to be followed-up. Extend the RV measurements on these targets will allow to refine the planetary parameters, to search for other planets in the systems, and to explore the magnetic activity of these stars. With orbital distance

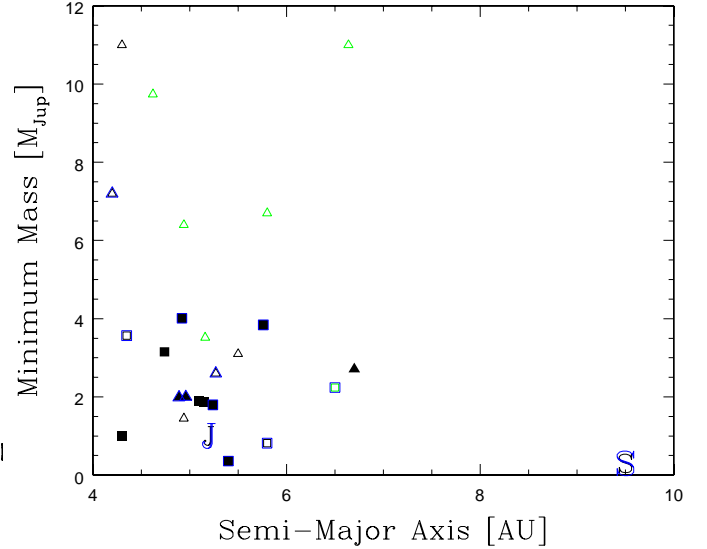


Fig. 12. Minimum mass as a function of the semi-major axis for planets detected by RV with $a > 4$ AU. Empty markers shows the incomplete orbits while filled ones represent complete orbits. Squares and triangles are, respectively, for low ($e < 0.25$) and high ($e > 0.25$) eccentricity orbits. The markers surrounded by blue show multiple systems. The green points shows the higher mass planets announced by Marmier et al. (in prep., private communication).

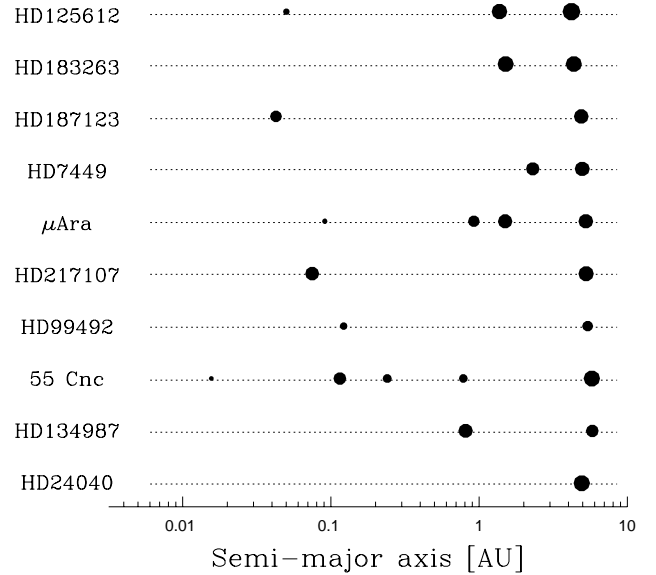


Fig. 13. Multiple systems with semi-major axis greater than 4 AU. The size of the dots shows the minimum mass of the planet in a log scale.

greater than 5 AU, imaging would be done to provide critical observational constraints on the system like its inclination and looking for outer bodies or to give spectral information about the planet. The candidates planets will engender an astrometric signature of hundreds of μas , for example, 550 μas on HD150706 and 175 μas on HD222155. Despite a duration mission with a shorter timescale than the orbital period, part of the orbit should be easily detected by Gaia. Moreover, these systems with long-period low-eccentricity Jupiter type planets may be similar to the

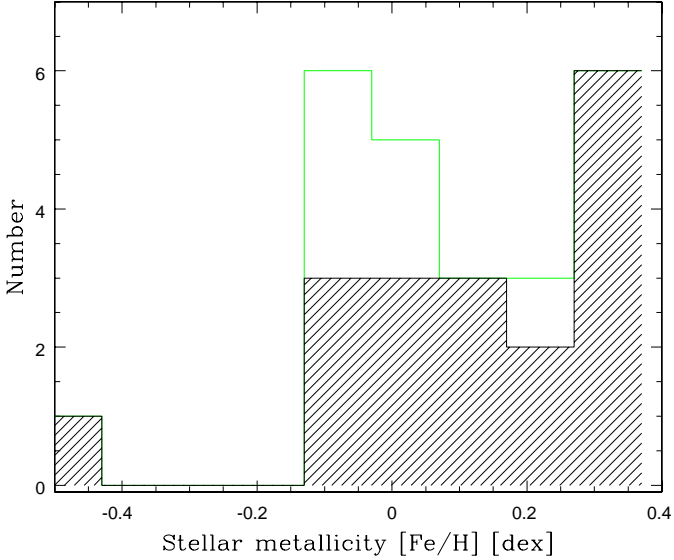


Fig. 14. Histogram of host star metallicities $[\text{Fe}/\text{H}]$ for the planets with semi-major axis greater than 4 AU (all are giant gaseous planets). In green, the histogram include the six candidates from Marmier et al. (in prep., private communication)

Solar System and may hold lower mass planets in shorter orbits like μ Ara (HD160691) and 55 Cnc (HD75732) systems. New fibers scramblers have been installed on SOPHIE (June 2011, Perruchot et al. 2011), and preliminary tests showed a significant improvement in the stability of the spectrograph illumination, and so, in the RV accuracy. These stars will then be followed-up with SOPHIE in order to search for multiplicity in these systems.

Hence, the transit probability for these candidates are very low, respectively, 0.07% and 0.16% for HD150706b and HD222155b. But, as they might host shorter period low-mass planets with higher transit probability, they are good targets to search for earth-like planets in transit around bright stars in order to find a Solar System twin.

Acknowledgements. The authors thanks all the staff of Haute-Provence Observatory for their contribution to the success of the ELODIE and SOPHIE projects and their support at the 1.93-m telescope. We thanks the referee for his/her careful reading and judicious comments. We wish to thank the “Programme National de Planétologie” (PNP) of CNRS/INSU, the Swiss National Science Foundation, and the French National Research Agency (ANR-08-JCJC-0102-01 and ANR-NT05-4-44463) for their continuous support to our planet-search programs. AE is supported by a fellowship for advanced researchers from the Swiss National Science Foundation (grant PA00P2_126150/1). IB and NCS would like to thank the support by the European Research Council/European Community under the FP7 through a Starting Grant, as well from Fundação para a Ciência e a Tecnologia (FCT), Portugal, through a Ciência 2007 contract funded by FCT/MCTES (Portugal) and POPH/FSE (EC), and in the form of grants reference PTDC/CTE-AST/098528/2008, PTDC/CTE-AST/098604/2008, and SFRH/BPD/81084/2011. DE is supported by CNES. This research has made use of the SIMBAD database and the VizieR catalogue access tool operated at CDS, France.

Appendix A: Constraining the RV offset between ELODIE and SOPHIE

When a star is observed by several instruments, the RV offsets between the different datasets are fitted as a free parameter in the Keplerian solution. A sample of about 200 stars, selected as stable from ELODIE measurements, have also been observed with SOPHIE in order to search for low-mass planets (Bouchy et al. 2009). This sample can be used to constrain the RV offset

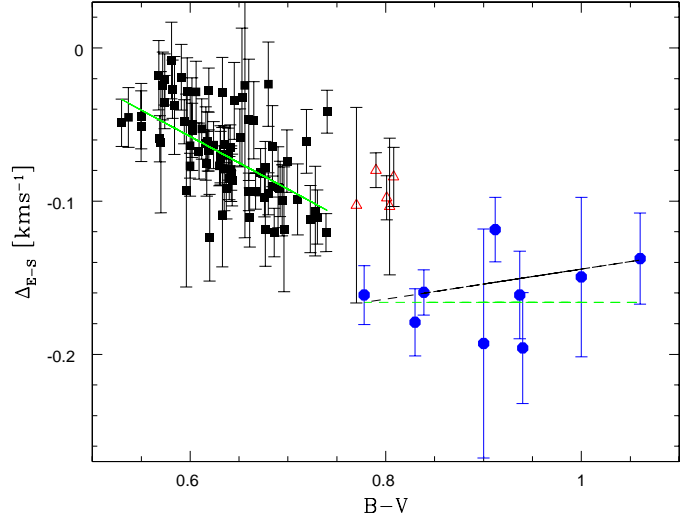


Fig. A.1. Difference between the mean RV from ELODIE and from SOPHIE, $\Delta(\text{RV})_{\text{E-S}}$ as a function of $B - V$ for a sample of stable stars. The error bars correspond to the quadratic sum of the standard deviation of ELODIE and SOPHIE RV data. The green solid line is the best linear fit for stars correlated with a G2 mask (black squares). Those with $B - V > 0.75$ are discarded (red triangles). The black dashed line is the best linear fit for stars correlated with a K5 mask (blue circles). The detection of the slope is not significant and a constant value is chosen (green dashed line).

between the two spectrographs as these stars have constant RV at the level of precision of ELODIE ($\sim 10 \text{ms}^{-1}$) on a timescale of several years. The Δ_{RV} is expected to depend on the color of the star ($B - V$) and at a second order (that we neglected) on its metallicity. With a mean value of 0.003 given by Hipparcos, we neglect the error on the $B - V$.

For both instruments, we compute the mean RV value for each star, $\text{RV}_{\text{ELODIE}}$ and $\text{RV}_{\text{SOPHIE}}$. The error bars correspond to the quadratic sum of the standard deviation of ELODIE and SOPHIE RV data. We then plot the difference $\Delta(\text{RV})_{\text{E-S}} = \text{RV}_{\text{ELODIE}} - \text{RV}_{\text{SOPHIE}}$ as a function of the $B - V$ in the Fig. A.1. The $\text{RV}_{\text{ELODIE}}$ are shifted into the blue compared to $\text{RV}_{\text{SOPHIE}}$. We consider separately the RV measurements derived from the G2 (black squares) and from the K5 (blue circles) cross-correlation mask.

With the K5 mask, a linear fit (black dashed line) is not well constrained and we chose a constant as an offset (green dashed line):

$$\Delta(\text{RV})_{\text{E-S}}(\text{K5}) = -166 \text{ms}^{-1} \quad (\text{A.1})$$

The residuals have a dispersion of 20ms^{-1} , value considered as our error on the RV offset.

With the G2 mask, stars with a $B - V > 0.75$ may have a different comportment than the others and should have been correlated with the K5 mask. This may be due to a bad spectral classification of these stars. We then fit a linear relation considering only the stars with $B - V < 0.75$ (green line):

$$\Delta(\text{RV})_{\text{E-S}}(\text{G2}) = -425.6(B - V) + 202.4 \text{ms}^{-1} \quad (\text{A.2})$$

The residuals around the fits is of 23ms^{-1} that we take as our offset calibration error.

On Fig. A.2, three stable stars observed during more than 13 yr are shown, illustrating the reliability of the calibration.

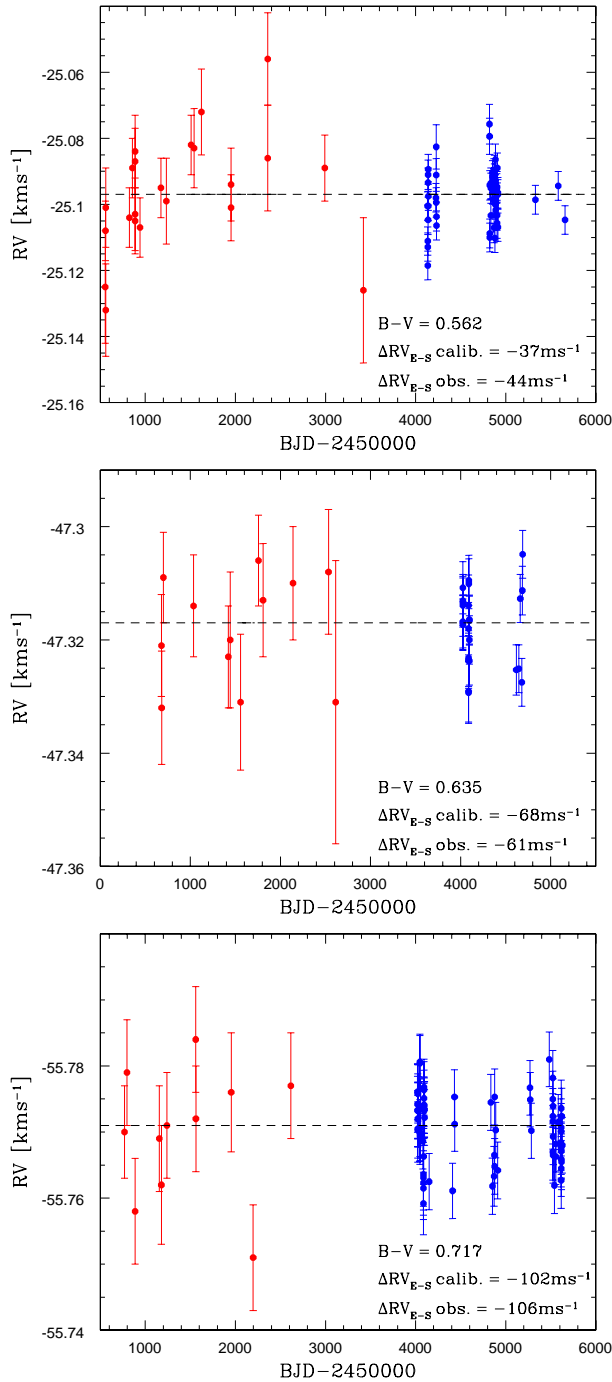


Fig. A.2. ELODIE (red points) and SOPHIE (blue points) RV of stable stars observed during more than 13 yr.

References

Allende Prieto, C. & Lambert, D.L. 1999, *A&A*, 352, 555
 Baliunas, S.L., Donahue, R.A., Soon, W.H. et al. 1995, *ApJ*, 438, 269
 Baranne, A., Queloz, D., Mayor, M., et al. 1996, *A&AS*, 119, 373
 Beckers, J.M. 2007, *AN*, 328, 1084
 Boisse, I., Moutou, C., Vidal-Madjar, A., et al. 2009, *A&A*, 495, 959
 Boisse, I., Bouchy, F., Chazelas, B., Perruchot, S., Pepe, F., Lovis, C., Hébrard, G. 2010a, in *New technologies for probing the diversity of brown dwarfs and exoplanets*, EPJ Web of Conferences, arXiv:1001.0794
 Boisse, I., Eggenberger, A., Santos, N.C. et al. 2010b, *A&A*, 523, 88B
 Boisse, I., Bouchy, F., Hébrard, G. et al. 2011, *A&A*, 528, A4
 Bond, I., Udalski, A., Jaroszynski, M. et al. 2004, *ApJ*, 606, L155
 Bouchy, F., Pont, F., Melo, C. et al. 2005, *A&A*, 431, 1105
 Bouchy, F., Hébrard, G., Udry, S. et al. 2009, *A&A*, 505, 853

Cumming, A. 2004, *MNRAS*, 354, 1165
 da Silva, L., Girardi, L., Pasquini, L. et al. 2006, *A&A*, 458, 609
 Diaz, R.F., Santerne, A., Sehlman, J. et al. 2012, *A&A*, 538, 113D
 Donati, J.-F., Moutou, C., Farès, R. et al., 2008, *MNRAS*, 385, 1179
 Dumusque, X., Lovis, C., Ségransan, D. et al. 2011, *A&A*, 535, 55D
 Duncan, D.K., Vaughan, A.H., Wilson, O.C. et al. 1991, *ApJS*, 76, 383
 ESA 1997, Online Data Catalog
 Farès, R., Donati, J.-F., Moutou, C. et al., 2009, *MNRAS*, 398, 1383
 Fischer, D. & Valenti, J. 2005, *ApJ*, 622, 1102
 Fischer, D., Marcy, G., Butler, R. et al. 2008, *ApJ*, 675, 790
 Fischer, D., Driscoll, P., Isaacson, H. et al. 2009, *ApJ*, 703, 1545
 Gonzalez, G., Carlson, M.K. and Tobin, R.W. 2010, *MNRAS*, 403, 1368
 Hébrard, G., Bonfils, X., Ségransan, D. 2010, *A&A*, 513, 69H
 Holmberg, J., Nordström, B. and Andersen, J. 2009, *A&A*, 501, 941
 Howard, A.W., Johnson, J.A., Marcy, G.W. et al. 2010, *ApJ*, 721, 1467
 Johnson, J.A., Clanton, C., Howard, A.W. et al. 2011, *ApJS*, 197, 26J
 Jones, H.R.A., Butler, R., Tinney, C. et al. 2010, *MNRAS*, 403, 1703
 Lo Curto, G., Mayor, M., Benz, W. et al. 2010, *A&A*, 512, 48L
 Lovis, C., Ségransan, D., Mayor, M. et al. 2011a, *A&A*, 528, 112
 Lovis, C., Dumusque, X., Santos, N.C. et al., arXiv:1107.5325
 Makarov, V. 2010, *ApJ*, 715, 500
 Mamajek, E. & Hillenbrand, L. 2008, *ApJ*, 687, 1264
 Marsakov, V.A. & Shevelev, Y.G. 1995, *BICDS*, 47, 13
 Masana, E., Jordi, C. and Ribas, I., 2006, *A&A*, 450, 735
 Masset, F. & Snellgrove, M. 2001, *MNRAS*, 320, 55
 Mayor, M. & Queloz, D. 1995, *Nature*, 378, 355
 Mayor, M., Marmier, M., Lovis, C. et al. 2011, arXiv:1109.2497
 Melo, C., Santos, N.C., Gieren, W. et al. 2007, *A&A*, 467, 721
 Meschiri, S., Laughlin, G., Vogt, S. et al. 2010, *ApJ*, 727, 117
 Meyer, M.R., Hillenbrand, L.A., Backman, D.E. et al. 2004, *ApJS*, 154, 422
 Morbidelli, A. & Crida, A. 2007, *Icarus*, 191, 158
 Moro-Martín, A., Carpenter, J.M., Meyer, M.R. et al. 2007, *ApJ*, 658, 1312
 Moutou, C., Mayor, M., Lo Curto, G. et al. 2011, *A&A*, 527, A63
 Naef, D., Mayor, M., Beuzit, J.-L. et al. 2005, *Proceedings of the 13th Cambridge Workshop on Cool Stars*, vol. 560, p.833
 Noyes, R.W., Hartmann, L.W., Baliunas, S.L., Duncan, D.K. and Vaughan, A.H. 1984, *ApJ*, 279, 763
 Pepe, F., Mayor, M., Galland, F., et al. 2002, *A&A*, 388, 632
 Pepe, F., Correia, A.C.M., Mayor, M. et al. 2007, *A&A*, 462, 769
 Perrier, C., Sivan, J.P., Naef, D. et al. 2003, *A&A*, 410, 1039
 Perruchot, S., Kohler, D., Bouchy, F. et al. 2008, in *Ground-based and Airborne Instrumentation for Astronomy II*, Edited by McLean, I.S., Casali, M.M., Proceedings of the SPIE, vol. 7014, 7014J
 Perruchot, S., Bouchy, F., Chazelas, B. et al. 2011, in *Techniques and Instrumentation for Detection of Exoplanets V*. Edited by Shaklan, Stuart. Proceedings of the SPIE, vol. 8151, 815115-12
 Rocha-Pinto, H.J., Flynn, C., Scalo, J. et al. 2004, *A&A*, 423, 517
 Robertson, P., Endl, M., Cochran, W.D. et al., arXiv:1202.0265
 Santos, N.C., Mayor, M., Naef, D., et al. 2000, *A&A*, 361, 265
 Santos, N.C., Israelian, G., Mayor, M. et al. 2003, *A&A*, 398, 363
 Santos, N.C., Israelian, G. and Mayor, M. 2004, *A&A*, 415, 1153
 Santos, N.C., Gomes da Silva, J., Lovis, C. and Melo, C. 2010a, *A&A*, 511, 54S
 Santos, N.C., Mayor, M., Benz, W. et al. 2010b, *A&A*, 512, 475
 Ségransan, D., Mayor, M., Udry, S. et al. 2011, *A&A*, 535, 54
 Sousa, S.G., Santos, N.C., Israelian, G., Mayor, M. and Monteiro, M.J.P.F.G. 2006, 458, 873
 van Leeuwen, F. 2007, *A&A*, 474, 653
 Wright, J.T., Marcy, G.W., Butler, R.P. and Vogt S.S. 2004, *ApJS*, 152, 261
 Wright, J.T., Marcy, G.W., Fischer, D.A. et al. 2007, *ApJ*, 657, 533
 Wright, J.T., Marcy, G.W., Butler, R.P. et al. 2008, *ApJ*, 683, 63
 Wright, J.T., Upadhyay, S., Marcy, G. et al. 2009, *ApJ*, 693, 1084
 Yee, J.C., Udalski, A., Subo Dong et al., arXiv:1106.4013

Table 1. Known exoplanets discovered by RV with orbital distance greater than 4 AU.

	Semi-major axis[AU]	Period [day]	Mass [M_{Jup}]	Ecc	Orbit*	Multiplicity [†]	ref.
HIP70849 b	4.5-36	5-90[yr]	3-15	0.47-0.96	incomp.	1	Ségransan et al. (2011)
HD150706 b	$6.7^{+4.0}_{-1.4}$ **	5894^{+5584}_{-1498}	$2.71^{+1.14}_{-0.66}$ **	$0.38^{+0.28}_{-0.32}$	incomp.	1	this paper
HD134987 c	5.8	5000±400	0.82±0.03	0.12±0.02	incomp.	2	Jones et al. (2010)
55Cnc d	5.76	5218±230	3.84±0.08	0.03±0.03	comp.	5	Fischer et al. (2008)
HD190984 b	5.5	4885±1600	3.1	0.57±0.10	incomp.	1	Santos et al. (2010b)
HD99492 c	5.4	4970±744	0.36±0.06	0.1±0.2	comp.	2	Meschiari et al. (2010)
HD217107 c	5.27	4270±220	2.60±0.15	0.517±0.033	incomp.	2	Wright et al. (2009)
μ Ara e	5.24	4206±759	1.8	0.10±0.06	comp.	4	Pepe et al. (2007)
HD13931 b	5.15	4218±388	1.88±0.15	0.02±0.05	comp.	1	Howard et al. (2010)
HD222155 b	$5.1^{+0.6}_{-0.7}$ **	3999^{+469}_{-541}	$1.90^{+0.67}_{-0.53}$ **	$0.16^{+0.27}_{-0.22}$	comp.	1	this paper
HD7449 c	4.96±0.30	4046±370	2.0±0.5	0.53±0.08	comp.	2	Dumusque et al. (2011)
HD24040 b	$4.92 \pm 0.38^{\Delta}$	3668^{+169}_{-171}	$4.01 \pm 0.49^{\Delta}$	$0.04^{+0.07}_{-0.06}$	comp.	1(+1?*)	this paper
HD220773 b	4.94±0.2	3725±463	1.45±0.3	0.51±0.1	incomp.	1	Robertson et al. (2012)
HD187123 c	4.89±0.53	3810±420	1.99±0.25	0.252±0.033	comp.	2	Wright et al. (2009)
HD72659 b	4.74±0.08	3658±32	3.15±0.14	0.22±0.03	comp.	1	Moutou et al. (2011)
HD183263 c	4.35±0.28	3070±110	3.57 ± 0.55	0.239±0.064	incomp.	2	Wright et al. (2009)
HD106270 b	4.3±0.4	2890±390	11±1	0.40±0.05	incomp.	1	Johnson et al. (2011)
HD154345 b	$4.3 \pm 0.4^{\Delta\Delta}$	3538±300	$1.0 \pm 0.3^{\Delta\Delta}$	0.26±0.15	comp.	1	this paper
HD125612 d	4.2	3008±202	7.2	0.28±0.12	incomp.	3 [‡]	Lo Curto et al. (2010)

* **comp.:** if the RV measurements cover the orbit; **incomp.:** if the RV measurements did not cover the orbit.

[†] give the number of planets **pl.** in the system. All planets, except HD125612b, orbit single stars.

* a linear trend is fit on the RV of this system.

[‡] HD125612A has a stellar companion

** assuming $M_{\star} = 1.17 \pm 0.12 M_{\odot}$

** assuming $M_{\star} = 1.13 \pm 0.11 M_{\odot}$

Δ assuming $M_{\star} = 1.18 \pm 0.10 M_{\odot}$

$\Delta\Delta$ assuming $M_{\star} = 0.88 \pm 0.09 M_{\odot}$

Table A.1. Radial velocities of HD 150706 measured with ELODIE.

BJD -2 400 000	RV (km s ⁻¹)	$\pm 1 \sigma$ (km s ⁻¹)
50649.4745	-17.194	0.009
50942.5543	-17.174	0.014
50970.5200	-17.196	0.012
50970.5325	-17.196	0.011
50972.5962	-17.197	0.010
50973.4466	-17.183	0.010
50973.4591	-17.178	0.012
51269.6057	-17.211	0.008
51723.4471	-17.189	0.009
51728.4541	-17.172	0.010
51757.4065	-17.189	0.008
52081.4290	-17.224	0.009
52113.4120	-17.255	0.008
52137.3848	-17.230	0.009
52160.3491	-17.198	0.013
52163.3009	-17.203	0.012
52360.6618	-17.243	0.012
52361.6448	-17.235	0.011
52384.6408	-17.227	0.013
52388.6133	-17.228	0.011
52414.5642	-17.250	0.009
52451.4536	-17.258	0.011
52451.4667	-17.244	0.012
52482.3970	-17.263	0.009
52508.3361	-17.243	0.010
52747.6042	-17.254	0.009
52748.5678	-17.247	0.009
52751.5813	-17.221	0.009
52752.5889	-17.224	0.008
52773.5429	-17.216	0.015
52774.5403	-17.228	0.018
52776.5571	-17.264	0.011
52778.5717	-17.245	0.008
52797.4581	-17.253	0.009
52800.5201	-17.238	0.009
52801.4400	-17.240	0.012
52803.4532	-17.253	0.009
52806.4494	-17.251	0.009
52809.4272	-17.243	0.010
52812.4224	-17.261	0.010
52813.4814	-17.262	0.009
53160.4959	-17.231	0.009
53164.4548	-17.236	0.010
53223.3977	-17.216	0.012
53486.6043	-17.214	0.011
53490.5529	-17.238	0.009
53517.5451	-17.237	0.009
53900.4554	-17.188	0.013

Table A.2. Radial velocities of HD 150706 measured with SOPHIE.

BJD -2 400 000	RV (km s ⁻¹)	$\pm 1 \sigma$ (km s ⁻¹)
54236.54555	-17.1770	0.0044
54600.60889	-17.1808	0.0043
54740.26854	-17.1806	0.0042
54889.64197	-17.1265	0.0043
55016.36337	-17.1479	0.0042
55050.48029	-17.1448	0.0042
55061.35488	-17.1510	0.0043
55063.33252	-17.1943	0.0043
55064.37769	-17.1777	0.0042
55066.32264	-17.0975	0.0043
55072.31036	-17.1709	0.0042
55074.31585	-17.1952	0.0042
55075.31406	-17.1521	0.0042
55076.31876	-17.1233	0.0043
55078.36177	-17.1370	0.0044
55079.33895	-17.1174	0.0043
55081.32237	-17.1624	0.0042
55088.34489	-17.1409	0.0042
55092.36418	-17.1885	0.0042
55096.38831	-17.1455	0.0043
55097.28451	-17.1610	0.0042
55098.28223	-17.1467	0.0043
55330.43771	-17.1678	0.0043
55331.48420	-17.1692	0.0043
55360.46481	-17.1541	0.0043
55361.44615	-17.1640	0.0042
55368.49765	-17.1355	0.0043
55379.47954	-17.1746	0.0042
55381.40204	-17.1568	0.0042
55383.40329	-17.1307	0.0043
55384.41523	-17.1591	0.0043
55391.39659	-17.1614	0.0043
55392.38517	-17.1462	0.0044
55395.38753	-17.1201	0.0043
55396.37419	-17.1606	0.0042
55397.37673	-17.1841	0.0042
55398.37019	-17.1750	0.0042
55399.38494	-17.1430	0.0042
55400.35673	-17.1436	0.0042
55401.35616	-17.1372	0.0044
55402.36160	-17.1653	0.0043
55403.37580	-17.1580	0.0043
55404.36871	-17.1336	0.0043
55405.34437	-17.1079	0.0043
55409.38627	-17.1421	0.0042
55424.34173	-17.1670	0.0042
55429.33811	-17.1585	0.0042
55476.30322	-17.1748	0.0042
55478.29437	-17.1674	0.0043
55479.26619	-17.1527	0.0043
55499.23547	-17.1677	0.0044
55527.23017	-17.1695	0.0045
55758.38710	-17.1495	0.0044

Table A.3. Radial velocities of HD 222155 measured with ELODIE.

BJD -2 400 000	RV (km s ⁻¹)	$\pm 1 \sigma$ (km s ⁻¹)
50675.6213	-44.001	0.008
50731.4575	-44.001	0.008
50767.3732	-44.013	0.008
50768.3859	-43.999	0.008
50773.4144	-44.018	0.009
51054.5803	-43.999	0.009
51054.5931	-44.008	0.010
51155.3039	-43.967	0.011
51422.5284	-43.972	0.008
51466.4467	-43.965	0.008
51506.4018	-43.988	0.008
51758.5948	-43.961	0.009
51835.4570	-43.973	0.008
51853.4017	-43.969	0.009
51858.3551	-43.974	0.008
51882.2985	-43.978	0.009
51906.3044	-43.978	0.010
52111.6150	-43.950	0.008
52112.6131	-43.964	0.007
52115.6158	-43.968	0.008
52116.6066	-43.969	0.008
52117.5774	-43.967	0.007
52136.5939	-43.978	0.008
52158.5965	-43.967	0.008
52159.5882	-43.980	0.009
52160.5985	-43.977	0.011
52161.3818	-43.975	0.010
52163.5326	-43.977	0.012
52164.5088	-43.953	0.008
52193.5460	-43.968	0.008
52194.4816	-43.979	0.007
52195.4841	-43.970	0.007
52197.4701	-43.964	0.009
52214.3879	-43.981	0.009
52252.3722	-43.970	0.009
52482.6168	-43.963	0.008
52510.5121	-43.966	0.010
52537.5497	-43.981	0.009
52855.6104	-43.990	0.008
52919.4593	-43.978	0.009
52923.4549	-43.993	0.008
52958.4170	-44.009	0.009
53626.4855	-44.009	0.009
53692.3277	-44.003	0.016

Table A.4. Radial velocities of HD 222155 measured with SOPHIE.

BJD -2 400 000	RV (km s ⁻¹)	$\pm 1 \sigma$ (km s ⁻¹)
54311.59377	-43.9328	0.0043
54313.60538	-43.9407	0.0042
54314.54313	-43.9498	0.0044
54316.55558	-43.9611	0.0042
54335.58083	-43.9366	0.0042
54337.58167	-43.9556	0.0042
54338.52044	-43.9831	0.0042
54344.49813	-43.9282	0.0043
54345.47122	-43.9441	0.0042
54346.50600	-43.9407	0.0042
54349.57894	-43.9281	0.0042
54358.54608	-43.9327	0.0042
54359.50478	-43.9434	0.0042
54360.50765	-43.9463	0.0042
54375.43443	-43.9516	0.0042
54404.38658	-43.9407	0.0043
54405.27033	-43.9362	0.0042
54406.32330	-43.9407	0.0041
54408.27384	-43.9490	0.0042
54408.28112	-43.9435	0.0042
54409.26993	-43.9646	0.0042
54409.27719	-43.9601	0.0042
54496.23763	-43.9132	0.0044
54497.24360	-43.9164	0.0043
54499.25691	-43.9183	0.0044
54514.26060	-43.9262	0.0043
54516.25281	-43.9195	0.0043
54644.60118	-43.9242	0.0043
54645.60320	-43.9364	0.0042
54646.59073	-43.9740	0.0042
54702.59379	-43.9050	0.0043
54724.51839	-43.9092	0.0042
55010.60439	-43.9120	0.0042
55050.49819	-43.9315	0.0042
55051.55869	-43.9412	0.0042
55054.62748	-43.9014	0.0045
55055.63100	-43.9253	0.0042
55056.54766	-43.9359	0.0042
55057.55794	-43.9428	0.0043
55058.53263	-43.9368	0.0046
55059.52953	-43.9370	0.0043
55061.54773	-43.9267	0.0042
55062.53034	-43.9242	0.0042
55063.56159	-43.9185	0.0042
55066.54844	-43.9091	0.0043
55072.48188	-43.9191	0.0043
55073.54251	-43.9047	0.0042
55391.58940	-43.9153	0.0042
55392.59350	-43.9250	0.0043
55393.60189	-43.9237	0.0042
55398.60598	-43.9220	0.0042
55400.61287	-43.9174	0.0042
55401.60001	-43.8956	0.0043
55402.58238	-43.9073	0.0042
55404.58194	-43.9056	0.0043
55405.51664	-43.9132	0.0042
55409.52903	-43.9464	0.0043
55433.57127	-43.9148	0.0042
55476.42251	-43.9267	0.0042
55478.43488	-43.9247	0.0042
55479.40630	-43.9083	0.0043
55483.45282	-43.9204	0.0042
55484.35799	-43.9226	0.0042
55495.44765	-43.9058	0.0044
55498.31985	-43.9354	0.0041
55505.38780	-43.9382	0.0042
55523.40552	-43.9088	0.0043

Table A.5. Radial velocities of HD 24040 measured with ELODIE.

BJD -2 400 000	RV (km s ⁻¹)	$\pm 1 \sigma$ (km s ⁻¹)
50701.66050	-9.458	0.008
50730.60090	-9.453	0.007
50732.61430	-9.452	0.008
50736.61110	-9.474	0.011
50890.32770	-9.473	0.010
51174.38940	-9.470	0.009
51238.26700	-9.466	0.008
51510.56610	-9.432	0.008
51951.35990	-9.393	0.008
52164.65860	-9.361	0.009
52194.59920	-9.360	0.008
52199.59010	-9.353	0.009
52214.58190	-9.353	0.012
52218.58010	-9.363	0.009
52220.53190	-9.364	0.015
52249.48790	-9.357	0.011
52278.40670	-9.362	0.010
52280.38100	-9.373	0.009
52308.36950	-9.366	0.008
52356.29560	-9.331	0.014
52361.29410	-9.326	0.017
52532.66570	-9.366	0.010
52559.61600	-9.347	0.011
52561.67100	-9.357	0.010
52565.62800	-9.355	0.010
52597.49410	-9.352	0.010
52637.41740	-9.380	0.010
52647.40080	-9.333	0.014
52677.32400	-9.339	0.019
52678.36200	-9.367	0.009
52679.34660	-9.315	0.017
52681.38730	-9.361	0.010
52856.62940	-9.370	0.009
52919.55000	-9.362	0.010
52922.59580	-9.363	0.008
52954.56470	-9.367	0.008
52958.50350	-9.362	0.011
52993.44400	-9.377	0.011
52996.40330	-9.347	0.020
53030.34120	-9.315	0.020
53034.37680	-9.335	0.013
53059.28940	-9.302	0.022
53358.41180	-9.363	0.016
53361.44080	-9.391	0.016
53421.30340	-9.389	0.025
53614.59350	-9.428	0.011
53726.40810	-9.416	0.011

Table A.6. Radial velocities of HD 24040 measured with SOPHIE.

BJD -2 400 000	RV (km s ⁻¹)	$\pm 1 \sigma$ (km s ⁻¹)
54503.29729	-9.3414	0.0043
54504.26177	-9.3422	0.0043
54505.26558	-9.3482	0.0043
54506.27614	-9.3425	0.0043
54507.30600	-9.3503	0.0043
54857.33346	-9.3258	0.0043
54872.32914	-9.3290	0.0043
55448.63161	-9.2676	0.0042
55476.65796	-9.2763	0.0042
55479.55853	-9.2716	0.0043
55483.55793	-9.2753	0.0042
55495.54768	-9.2659	0.0043
55519.49131	-9.2764	0.0042

Table A.7. Radial velocities of HD 89307 measured with ELODIE.

BJD -2 400 000	RV (km s ⁻¹)	$\pm 1 \sigma$ (km s ⁻¹)
50796.70270	23.059	0.009
50822.59530	23.030	0.009
50823.59750	23.032	0.009
50824.59000	23.039	0.009
50859.52380	23.045	0.009
50888.48800	23.021	0.010
50888.50040	23.022	0.010
50908.39060	23.032	0.009
50942.37900	23.019	0.009
50972.34880	23.010	0.009
51153.72040	23.056	0.012
51177.62610	23.041	0.010
51234.51360	23.007	0.010
51507.69750	23.053	0.009
51562.57770	23.059	0.013
51623.44230	23.024	0.010
51626.41540	23.049	0.011
51655.37180	23.055	0.010
51953.65880	23.129	0.017
51954.57500	23.070	0.012
51955.52670	23.072	0.011
51956.49000	23.075	0.010
51978.48600	23.022	0.033
51979.46550	23.038	0.011
52007.35270	23.096	0.012
52008.38870	23.082	0.013
52009.47000	23.060	0.019
52010.43190	23.056	0.013
52033.36360	23.102	0.014
52038.38040	23.071	0.010
52248.71710	23.164	0.025
52248.72820	23.138	0.015
52252.68720	23.103	0.016
52252.70430	23.109	0.011
52356.44340	23.085	0.019
52356.45680	23.133	0.018
52358.43760	23.117	0.011
52388.41390	23.070	0.010
52649.68980	23.044	0.015
52677.55470	23.068	0.011
52719.43880	23.050	0.008
52996.58680	23.060	0.015
53726.63150	23.083	0.013
53750.72660	23.075	0.016
53756.57870	23.050	0.014
53842.36680	23.081	0.013

Table A.8. Radial velocities of HD 89307 measured with SOPHIE.

BJD -2 400 000	RV (km s ⁻¹)	$\pm 1 \sigma$ (km s ⁻¹)
54097.67291	23.1332	0.0043
54097.68020	23.1324	0.0043
54889.51926	23.1348	0.0043
54904.50409	23.1351	0.0045
55238.50655	23.1079	0.0045
55267.54064	23.1007	0.0046
55525.68715	23.0984	0.0043
55526.70981	23.0989	0.0044
55527.67595	23.0979	0.0042
55586.56773	23.0925	0.0043
55615.48424	23.1047	0.0044

Table A.9. Radial velocities of HD 154345 measured with ELODIE.

BJD -2 400 000	RV (km s ⁻¹)	$\pm 1 \sigma$ (km s ⁻¹)
49464.62350	-46.955	0.008
49465.61330	-46.972	0.007
49527.49660	-46.966	0.007
49530.57980	-46.943	0.013
49611.28600	-46.986	0.008
49612.33000	-46.947	0.010
49753.70470	-46.960	0.007
49824.57510	-46.970	0.008
49905.46200	-46.968	0.009
50026.25970	-46.960	0.011
50210.55670	-46.983	0.007
50265.48900	-46.973	0.008
50651.40100	-46.954	0.009
50943.59820	-46.948	0.008
51357.44270	-46.951	0.009
51693.49520	-46.927	0.009
51755.38700	-46.940	0.008
51805.33550	-46.929	0.011
52080.46120	-46.928	0.008
52081.45600	-46.934	0.007
52136.38430	-46.931	0.007
52195.27040	-46.930	0.007
52217.23170	-46.924	0.008
52357.64990	-46.932	0.011
52385.56940	-46.927	0.009
52415.44280	-46.921	0.008
52459.46540	-46.923	0.009
52513.39240	-46.947	0.012
52513.40130	-46.938	0.009
52723.67010	-46.947	0.008
52772.62020	-46.922	0.007
52922.27230	-46.935	0.007
53160.51780	-46.955	0.008
53275.27350	-46.948	0.008
53275.35870	-46.960	0.010
53276.27840	-46.954	0.009
53277.33430	-46.958	0.008
53278.26730	-46.947	0.009
53278.36430	-46.971	0.009
53280.26290	-46.964	0.008
53280.33920	-46.957	0.009
53281.25430	-46.954	0.008
53281.33470	-46.966	0.008
53490.57280	-46.950	0.008
53516.60050	-46.964	0.008
53845.61620	-46.955	0.013
53898.53400	-46.969	0.009
53900.47320	-46.953	0.009
53935.45520	-46.981	0.008

Table A.10. Radial velocities of HD 154345 measured with SOPHIE.

BJD -2 400 000	RV (km s ⁻¹)	$\pm 1 \sigma$ (km s ⁻¹)
54261.50985	-46.8984	0.0042
54515.70527	-46.8432	0.0042
54539.69224	-46.8375	0.0042
54647.44384	-46.8425	0.0043
55268.65075	-46.8275	0.0041
55272.64768	-46.8235	0.0041
55391.38714	-46.8314	0.0042
55448.30372	-46.8162	0.0042
55619.69751	-46.8187	0.0042
55671.61674	-46.8318	0.0042
55671.62197	-46.8391	0.0042